Size-selective mortality may trigger maladaptive changes of shoaling behaviour in a fish

Valerio Sbragaglia[a,b,1,2], **Pascal P. Klamser**[c,d,1], **Pawel Romanczuk**[c,d,3], **and Robert Arlinghaus**[a,e]

[a]Department of Biology and Ecology of Fishes, Leibniz-Institute of Freshwater Ecology and Inland Fisheries, Müggelseedamm 310, 12587 Berlin, Germany
[b]Department of Marine Renewable Resources, Institute of Marine Sciences (ICM-CSIC), Barcelona, Spain
[c]Department of Biology, Institute for Theoretical Biology, Humboldt-Universität zu Berlin, 10115 Berlin, Germany
[d]Bernstein Center for Computational Neuroscience, 10115 Berlin, Germany
[e]Division of Integrative Fisheries Management, Department of Crop and Animal Sciences, Faculty of Life Science, Humboldt-Universität zu Berlin, Invalidenstrasse 42, 10115 Berlin, Germany

Size-selective mortality is a major evolutionary driver in fishes. Human-induced changes in size-selective mortality may trigger individual behavioral changes, which in turn may affect collective behavior. Studying the cause-and-effect of size-selective mortality is challenging in the wild, but insights can be gathered through experimental evolution in the laboratory. Previous results from a multi-generation harvest selection experiment with zebrafish (*Danio rerio*) as a model species showed that size-selective mortality affected group risk-taking behavior. We investigated a possible link between group risk-taking behavior and shoal cohesion in response to large (typical of most wild capture fisheries targeting larger size classes) and small (typical of specialized fisheries and gape-limited predators targeting smaller size classes) size-selective mortality. We document a negative relationship between group risk-taking behavior and shoal cohesion. We also propose a mechanistic explanation for this counter-intuitive finding through an increase in vigilance towards environmental cues at the expense of attention paid to social cues in response to large size-selective mortality (and vice versa for small size-selective mortality). Agent-based model simulations further revealed that the changes of collective behavior in response to large size-selective mortality might be adaptive under fishing scenarios by decreasing exploitation rate. By contrast, the same collective behavior favored by large size-selective mortality might be maladaptive in the presence of predation and increased natural mortality. The harvesting-induced changes we documented may slowly, but steadily erode the natural adaptive value of shoaling behavior in many species targeted by global fisheries.

boldness | **cohesion** | **collective** | **vigilance** | **evolution** | **fishing** | **predation**

[1] V.S. and P.P.K. contributed equally to this work.

Correspondence:

[2]experimental data: valeriosbra@gmail.com

[3]models and simulations: pawel.romanczuk@hu-berlin.de

Contributions:

V.S. and R.A. designed the experiments; V.S. performed the experiments, the statistical test and analysed part of the experimental data. P.P.K. and P.R. developed the model. P.P.K. ran the simulations and analyzed part of the experimental data. V.S., P.P.K., P.R. and R.A. interpreted the data. V.S., P.P.K, P.R. and R.A. wrote the manuscript. All authors have agreed to all manuscript contents.

Introduction

Size-selective mortality is a major evolutionary driver in fishes, which usually suffer a higher rate of natural mortality at juvenile than adult stages (1, 2). Human activities can profoundly alter the natural, mortality-based fitness landscape. A prime example is fishing, which can disproportionally increase adult mortality at a speed hardly ever experienced in the evolutionary history of most exploited fish populations (3). Another example could be an invasive predator selectively preying upon smaller individuals as showed for the lionfish, *Pterois miles*, in the Mediterranean Sea (4), or diseases released from temperature constraints due to climate change (5), which could affect specific size classes. Therefore, human-induced changes in size-selective mortality can be widespread in aquatic ecosystems and trigger adaptive responses in terms of life-history as well as physiological and behavioural traits, as suggested for intensive and size-selective harvesting (6–8). However, as in many evolutionary contexts (9), the understanding of possible maladaptive processes in response to size-selective mortality has been largely overlooked (but see 10).

Behavioural adaptations in response to size-selective mortality are particularly important because they might determine the success or failure of organisms in response to human-induced environmental changes (11–13). In this context, collective behaviour could be important because many fish species form shoals, which have a strong natural adaptive value by reducing predation risk and increasing foraging efficiency (14–16). Moreover, collective behavior such as shoaling could also be under selection by human activities such as fishing. Indeed, shoaling behaviour is a key driver of the capture process (17). Considering that collective behavior shown rapid evolution in response to artificial selection (18), fisheries-induced evolution can move the fitness landscape of collective behavior away from the natural optimum as shown for life history traits (3). Therefore, fishing could be a suitable example to understand the mechanisms governing the adaptive as well as maladaptive consequences of collective behaviour in response to human-induced changes in size-selective mortality.

The emergence of collective behaviour in fish and other an-

DRAFT

imals can be explained by simple interactions rules among individuals that are influenced by their respective neighbours (19–21). Major group-level behavioural transitions can be triggered by minor changes in social interactions at the individual level (22). Therefore, human-induced evolution could affect collective behaviour, such as shoaling, by changing individual behavioural traits that influence the interactions rules that drive group behaviour. For example, fish are expected to evolve reduced individual risk-taking behaviour in response to exploitation by passive fishing gears (6, 23), which in turn could reduce collective performance such as shoaling (24). However, the mechanisms governing fisheries-induced evolution of individual behaviour are poorly understood (3, 25), and the role of evolutionary changes of individual behaviour in driving collective behaviour is largely unexplored in a fishing as well as other human-induced evolutionary context.

Several mechanisms could shape how evolution of individual behavioural traits in response to size-selective mortality may affect collective behaviour. For example, heterogeneity of individual behaviour can play an important role in driving collective behavioural outputs such as shoal cohesion (26), as shown in qingbo, *Spinibarbus sinensis*, where shoals composed of either exclusively shy or bold individuals were less cohesive than shoals formed by individuals with a diversity of boldness levels (27). Also slow individual swimming speed increases shoal cohesion as shown for different fish species (27–29). In addition, shoal cohesion may be affected by a trade-off between vigilance (i.e. the frequency of environmental scans), and the use of social cues within a shoal. Empirical evidences for this trade-off are reported for three-spined sticklebacks, *Gasterosteus aculeatus* (more aligned individuals responded slower to an external cue; 30), or for herring, *Clupea harengus* (solitary individuals responded faster to an external cue than schooling individuals; 31). Vigilance can be affected by group size (32–34) or social behaviour (e.g. territorial aggression; 35). How vigilance influences cohesion is to our knowledge largely unexplored in general and in a size-selective mortality context. For example, shoals predominantly composed of individuals with reduced risk-taking behaviour – i.e. shy individuals, which is an adaption predicted in fisheries-induced evolution under large size-selective harvesting (6) - might be more vigilant (36, 37) at the expense of paying less attention to their conspecifics, in turn reducing shoal cohesion. Considering that individual fish risk-taking behaviour is expected to evolutionary change in response to size-selective mortality (6), important effects on shoaling behaviour are likely (38), but a mechanistic explanation is still missing. Moreover, while evolutionary changes of shoaling behaviour are expected to be adaptive in the new human-induced size selective mortality scenario (e.g., increased survival in a fishing context), it is an open question whether such changes might become maladaptive in a natural fitness landscape (e.g., decrease survival in a natural predation context).

We take advantage of a long-term harvesting experiment of zebrafish as a model shoaling species. Experimental lines were subjected to five generations of opposing size-selective mortality (39): large-harvested line (larger individuals harvested; a common scenario in many fisheries worldwide and in presence of predators where large individuals are selectively preyed upon), small-harvested line (smaller individuals harvested; a possible scenarios in specific fisheries or in the presence of gape-limited predators that preferentially feed on the smaller size classes) and random-harvested line (control). Previous results revealed substantial changes in life history, body size, gene expression, allele frequencies as well as individual and group behavioural traits (39–44). In particular, size-selective mortality affected risk-taking behaviour (42). Therefore, this experimental system has potential to explore the link between risk-taking and shoaling behaviour and the emergence of possible adaptive or maladaptive processes in response to size-selective mortality.

Zebrafish increase shoal cohesion in the presence of predation risk (45, 46). Therefore, an increase in risk-taking behaviour (i.e., a decrease in vigilance) should result in individuals forming less cohesive shoals because of a decreased in sensitivity to predation risk. Accordingly, we predicted that the increase in group risk-taking behaviour observed in the small-harvested line would be linked to a decrease in shoal cohesion (vice versa for the large-harvested line; Fig. 1). Although risk-taking behaviour has been measured as the time spent feeding at the water surface under the risk of predation (42), zebrafish respond to predation risk by both reducing shoal cohesion and spending more time at the bottom of the tank (45), which links these two behaviours. Next, to fully understand the mechanistic process driving the possible differences in shoal cohesion among the selection lines, we developed an agent-based model that relates individual-level traits (e.g., swimming speed and burst rate using environmental vs. social cues) to group-level emergent properties (Fig. 1). We used high resolution tracking of individual fish within groups to calibrate the burst-coast-agent-based model. Lastly, with the model representations of the selection lines, we simulated the collective behaviour in the presence of a natural predator or fishing gear to explore the adaptive and maladaptive response in natural and human-shaped evolutionary contexts (Fig. 1). In summary, our paper presents novel experimental data on the possible evolutionary changes in shoal cohesion as well as theory to mechanistically explain our findings. The results are synthesized through simulations to predict the effects of size-selective harvesting in fishing as well as natural predation scenarios.

Methods

A. Selection lines. Our study system consisted of wild-collected zebrafish from West Bengal in India (for more details see 44, 47). The parental wild-collected population was experimentally harvested over five generations (39) by exposing them to strong directional selection (a harvest rate of 75 percent per-generation) for either small body size (large-harvested line) or large body size (small-harvested line). A third line was harvested randomly with respect to size and used as a control (random-harvested or control line). Each

DRAFT

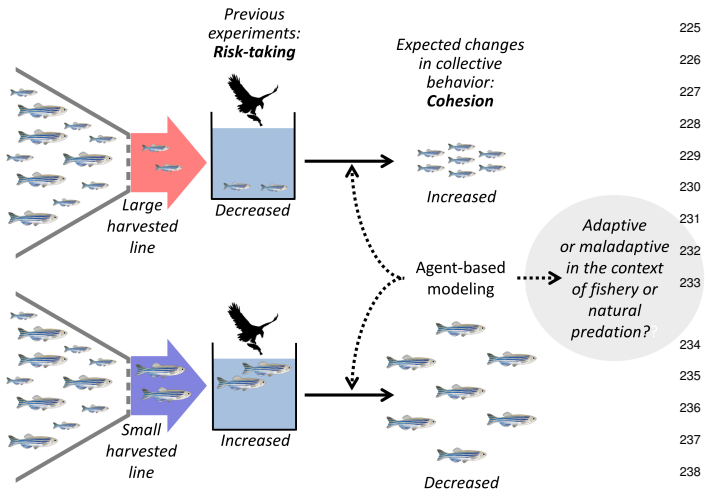

Fig. 1. The conceptual framework used in our study. Previous experiments showed that size-selective harvesting triggered changes in collective risk-taking by showing a strong decreasing trend in the large-size selective line and increasing it in the small-harvested line compared to controls (42). The solid arrows represent the experimental hypotheses tested in our study. Note that changes in shoal cohesion are expected relative to controls in both size-selected lines. Next, we calibrated an agent-based model to mechanistically understand the process driving the resulting collective phenomena (dotted arrows). Finally, we used the model to simulate different fishing and natural predator scenarios to explore adaptive or maladaptive value of changes in collective behavior. Zebrafish pic source: https://commons.wikimedia.org; Bird pic source: https://www.piqsels.com

selection line was replicated twice, which adds up to six selection lines. After five generations the harvesting was stopped for eight further generations until F13 – a time when the present experimental trials took place. At F9 the large-harvested line evolved a smaller adult length and weight and higher relative fecundity compared to controls (39). By contrast, the small-harvested line showed reduced reproductive investment and no change in adult length compared to the control line (39). Both size-selected lines matured smaller and at younger age than the control line (for more details see 39). These differences persisted until F13 (40, 41). Overall, the size-selective mortality triggered changes in energy allocation patterns, with the large-harvested line investing early and intensively into reproduction, and the small-harvested line investing early but at low intensity into gonad production and more intensively in somatic growth.

B. Experimental design. We stocked 8 juvenile zebrafish at 30 days post fertilization from each of the six selection lines into three-liter rearing boxes. The fish groups were the same os those used to measure group risk-taking behavior (42), but at different times (risk-taking behavior was measured at 230-240 days post fertilization, while the experiments presented here were at 190 days post fertilization). We randomly selected 6 groups of 8 individuals from each selection line (N=12 groups per selection treatment). The groups were housed in random order on shelves of the same holding system. Throughout the experiment zebrafish were fed ad libitum with dry food (TetraMin, Tetra), the water temperature was maintained at 26±0.5 °C and photoperiod at 12:12 h light-darkness cycle (light on/off at 07:00 and 19:00, respectively). All trials were run between 09:00 and 14:00. We started the experimental trials two hours after light-on to avoid measuring mating behavior that usually occurs in the first hours after light-on (48). The movement of the fish from the rearing boxes to the experimental tanks was conducted by gently pouring them together with the water from the stocking box. The experimental protocols were approved by the Spanish National Committee and the Committee of the University of Murcia on Ethics and Animal Welfare (CEEA-OH 491/2019).

C. Shoaling experiment. We measured shoaling behavior in groups of 8 zebrafish in a white round arena (diameter of 49 cm) with 10 cm of water. The arena was placed on a table behind a white curtain to minimize disturbance to the fish during the experimental trials. We recorded behavior using a webcam (resolution: 1920 x 1080 pixels; frame rate: 30 frames per second) from about 1m above the arena. Zebrafish were introduced in the experimental arena and left undisturbed for 25 min before starting the experimental trial. Video recording lasted 5 min and after that we measured the standard length of each fish on a petri dish with millimeter paper anesthetizing the fish using a clove oil dilution in ethanol and water. We analyzed the video recordings with the idTracker software. The software extracts specific characteristics of each individual and uses them to identify each fish without tagging (49).

D. Data analysis. We characterized shoaling behavior according to three group-level variables: inter-individual distance (i.e., the average distance of a given fish from all the other fish in the arena), nearest-neighbor distance (i.e., the distance from a focal fish to its closest neighbor averaged over all fish), and polarization (i.e, the absolute value of the mean heading direction). We only considered the frames where all the shoal members were detected (30 out of the 36 trials were used; N = 10 for each line treatment). Moreover, we calculated individual-level variables such as speed and burst rate. In this case, the output of the behavioral tracking was filtered by excluding frames with a probability of correctly identifying an individual below 0.85. This increased the tracking quality, but reduced the number of trials used in the individual analysis (18 out of the 36 trials were used; N = 6 for each line treatment). The modelling approach explained below focused on burst and coast phases, therefore individual identification was vital because properties of the burst phase, as its duration and rate, can be corrupted by tracking inaccuracy. Assuming that the remaining inaccuracy was random, we used a moving average with a Gaussian kernel to correct it (Figs. S7, S6).

E. Statistical approach for behavioral data. Group (inter-individual distance, nearest-neighbor distance, and polarization) and individual (body size, speed and burst rate) measurements were transformed when necessary by finding the exponent (λ), which made the values of the response variable as normally distributed as possible with a power transformation. Then, response variables were modelled using lin-

DRAFT

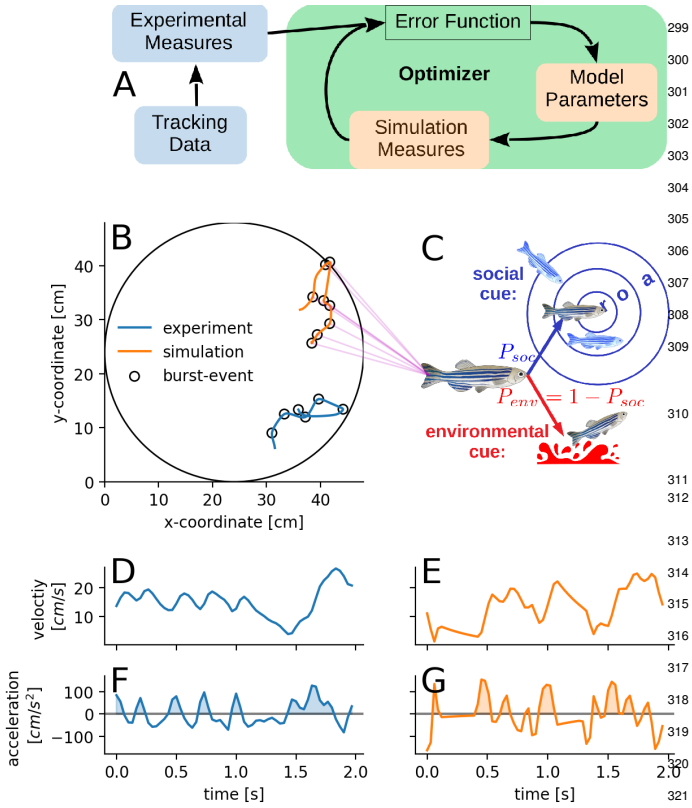

Fig. 2. A scheme of the model parameter estimation used here. The green rectangle represents the optimizer, which updates the model parameters. The update runs until the error function, which compares experimental with simulated measures, is minimal (**A**). The round arena shows representative experimental (blue) and simulation (orange) trajectories of an individual of the random harvested line together with detected burst events (circles; **B**). The schematic model description shows that at each burst an individual can follow with probability P_{soc} social cues (i.e. behaves according to a three-zone model: r=repulsion-, o=orientation-, a=attraction-zone) or with probability $P_{env} = 1 - P_{soc}$ environmental cues (**C**). The plots show velocity and acceleration of representative experimental (**D, F**) and simulated (**E, G**) trajectories.

ear mixed effects models with selection lines as fixed effect and selection line replicate as random intercepts. Likelihood ratio tests were used to assess the significant effect of selection lines as fixed effect (95 % confidence interval). Considering that zebrafish individual behavior is correlated with size (50) and that the size-selective treatments modified the size at age of the selection lines (39), it is conceivable that individual size differences among the selection lines could have masked harvesting-induced changes in terms of individual behavior. We thus estimated the effect of size (standard length) as a covariate against individual behavior. We implemented a second set of models with a size-matched dataset. The response variables were modelled by using linear mixed models and implementing all possible models (i.e., four) with individual body length as covariate, selection lines as fixed effect and selection line replicate as random intercepts. Likelihood ratio tests were used to assess the significant effect of selection lines and body length (95 % confidence interval).

All statistical analysis were implemented using R 3.5.0 (https://www.R-project.org/).

F. Shoaling model (burst and coast model). To unravel the mechanistic underpinning of our empirical results, we implemented a burst-coast-agent-based model (Fig. 2; Movie S1). We reproduced the zebrafish typical burst-coast swimming by a burst phase, initiated at a rate γ, in which a fish i accelerates along a constant force ($\vec{F}_i$) for the duration of the burst (t_b). If the fish does not burst, it coasts (i.e. its acceleration force is zero $\vec{F}_i = 0$) by decelerating due to friction (friction coefficient β) and keeps its heading direction ($\hat{e}_{\parallel,i}$). This behavior corresponds to the changes in position $\vec{r}_i$ and velocity $\vec{v}_i$ according to

$$\frac{d\vec{r}_i}{dt} = \vec{v}_i \ , \quad \vec{v}_i = v_i(\cos\varphi_i, \sin\varphi_i)^T = v_i \hat{e}_{\parallel,i} \qquad \textbf{(1)}$$

$$\frac{dv_i}{dt} = -\beta v_i + F_{\parallel,i}, \quad \frac{d\varphi_i}{dt} = \frac{1}{v} F_{\perp,i} \qquad \textbf{(2)}$$

with v_i and φ_i being the fish speed and its heading direction, which are altered by the force components parallel $F_{\parallel,i}$ and perpendicular $F_{\perp,i}$ to the heading direction $\hat{e}_{\parallel,i}$, respectively (51).

During each burst, the fish decides whether to react to social (i.e., other conspecifics) or random environmental cues with probability P_{social} and $1 - P_{social}$, respectively. The reaction strength $F = |\vec{F}|$ is in both cases the same, only the force direction distinguishes them. The social force direction $\hat{f}_{soc}$ is implemented according to a well-established three-zone model (22). A fish reacts by turning away to avoid collisions at short distances $r < r_r$, by aligning at intermediate distances $r_r < r < r_o$, and by being attracted at large distances $r_o < r < r_a$ (Fig. 2C). The direction of the alignment force of fish i is the sum of the velocity differences $\vec{v}_{ji} = \vec{v}_j - \vec{v}_i$ to its nearest neighbors in the alignment zone. We assume interactions with the first shell of nearest neighbors (Voronoi neighbors 52). If multiple zones are occupied including the repulsion zone, alignment- or attraction neighbors are ignored. Otherwise, the force direction is the weighted average of the alignment- and attraction-direction. The weights are the number of fish in the respective zone.

The environmental force direction $\hat{f}_{env}$ is random if no threat is detected (see Sect. G for possible threats). This is motivated by the fish misinterpreting non-controllable random perturbations (e.g. water reflections) as a threat and responding to them accordingly.

Additional parameters describing the repulsion force from the wall are avoided by a parameter free wall-avoidance mechanism ensuring that the fish avoids the wall while pursuing its intended direction (Movie S2, see SI for details).

F.1. Parameter setting. For the model to resemble the experimental data (Fig. 2B, D, E, F, G) we directly measured the parameters if possible, or minimized the error of the simulations with respect to experimental data via an optimizer (Fig. 2A). Six of the eight parameters were inferred from experimental data without the need to explicitly run model-simulation. The remaining two were set by repeatedly simulating the model and reducing the error to the experimental values of the group structure (i.e. NND) and the individual dynamics (i.e. average individual speed), as described below

DRAFT

(Fig. S2). We aimed at explaining the differences in NND between the selection lines. Since any of the eight parameters could contribute to the differences, we estimated each parameter for each selection line separately. However, the friction coefficient is assumed to be the same for all lines because it is not behavior dependent and size effects are negligible (see SI Sect. II. A).

The simulation-free parameter estimation was possible for the friction coefficient β, burst-rate γ and -duration t_b and for the range of each social zone (r_r, r_o, r_a). We split individual trajectories in burst and coast phases. A burst phase of a shoaling fish is characterized by an increase in its speed. The friction coefficient β is the deceleration during coast phases (Fig. S5). $\langle t_b \rangle$ was the mean burst length and $\langle \gamma \rangle$ the mean number of burst events per time unit. However, they are different from the model parameters t_b and γ. Burst events can overlap each other and consequently reduce the measured burst rate and prolong its duration (Fig. S2D). By a simple binary time series generating model we took account for this effect (See SI Sect. II. A).

We set the range of each social zone by minimizing the angle (error) between the predicted and the experimentally observed direction after a burst (Fig. 2A, SI Sect. II. A). The predicted burst direction of a fish is the social force direction computed from its neighbors relative position and velocity (See SI Sect. II. A).

A simulation-based parameter estimation was necessary for the burst force F and the probability to respond to social cues P_{soc}. We minimized the squared differences (error) between the simulated and experimentally observed values of the nearest-neighbor distances and the average individual speeds. Both measures are emergent properties of the model which require its explicit simulation (Fig. 2A). The differences were standardized by their experimental standard deviation (SI Sect.II. B). We restricted the search space by setting lower and upper bounds for the parameters(see SI Sect. II and Tab. S2). We did not minimize the error to the experimental polarization because (i) it does not differ between selection lines, (ii) the width of the orientation zone, mostly influencing the polarization, is already estimated from data, (iii) boundary effects could affect it (i.e., fish might be attracted to the wall but avoid it at close ranges, which could lead to a confounding alignment with the wall). For the minimization we applied the covariance matrix adaptation evolution strategy (CMA-ES; (53)), from the Python package *pycma* (54) which is a good choice for a multi-modal, noisy error-landscape.

G. Predator and fishing simulations.

We used the agent-based model representations of the three selection lines to investigate whether the size-selective harvest could impact the ability of the shoals to evade a natural predator and different fishing gear. We simulated $N = 30$ shoaling fish in a box of size $L = 100\ cm$ with periodic boundary conditions. Three scenarios were considered: (i) natural predation - including the confusion effect (55) - by a single mobile predator following the closest fish; (ii) fishing by a single agent without information about the position of the shoal (random search, similar to a fisher on a boat without an echo sounder); (iii) fishing by multiple aligned agents moving on a straight line towards the center of mass of the shoal (e.g., commercial trawling informed on the position of the shoal).

In contrast to the simulation with only shoaling fish, now the environmental force direction $\hat{f}_{env}$ is given by a direct avoidance force (repulsion) away from the simulated predator/fishing agent, if it is detected. The detection probability is maximal up to the detection distance $r_f = 7\ cm \approx 3BL$, and it decays linearly until it equals zero at $r = 35\ cm \approx 14BL$. All additional parameters for the three scenarios are explained below (summarized in Tab. S3).

G.1. Natural predator. The predator moves directly to the closest fish (Movie S3) with $v_{net} = 20,\ 25,\ 30,\ 35\ cm/s$, which is larger than the average speed of shoaling fish ($\langle v \rangle \approx 15\ cm/s$) because predators are usually larger than prey and therefore can swim faster (56, 57). Most predators attack a specific fish and therefore need to focus on it before attacking. The so-called confusion effect (58), the disruption of the predator focus by a large number of individuals who are difficult to distinguish by phenotype and movement, is believed to be one key benefit of group living (15). We model the probability of a prey to be successfully captured if it is closer to the predator than $r_{capture} = 5cm$ within a small time window $[t, t+\delta t]$ as

$$p_{success,i}(t, \delta t) = p_{confuse}(t) \cdot \gamma_a \delta t \qquad \textbf{(3)}$$

Here $\gamma_a = 1/s$ is a base predator attack rate and $p_{confuse}(t)$ represents the confusion effect that modulates the attack rate. The confusion term decreases $p_{success}$ with increasing number of perceived prey N_{sensed} in a sigmoidal fashion (see SI sect.I. D). Thereby, $N_{conf} = 4$ is the number of sensed shoaling fish at which $p_{confuse} = 0.5$ (58), and a fish is sensed if it is closer than $r_{sense} = 4r_{capture}$.

G.2. Fishing agents. Fishing agents always capture a shoaling fish if it is closer than $r_{capture} = 5\ cm$. Fishing gears were simulated by varying the speed of the fishing agents ($v_{net} = 7.5,\ 15,\ 22.5\ cm/s$).

In the single fishing agent scenario (Movie S4), the agent performs a random search with constant speed v_{net}. Its angular change is given by $d\varphi/dt = \hat{\sigma}_\varphi \xi(t)$ with $\xi(t)$ as white noise. For different speed values the angular noise strength $\hat{\sigma}_\varphi$ is adapted such that the persistence length is constant $\hat{\sigma}_\varphi = \sigma_\varphi \sqrt{v_{net}}$, i.e. the change in angle after travelling a certain distance is independent of its velocity (see SI sect.I. E).

In the multiple aligned fishing agents scenario (Movie S5), the agents ($N_f = 50$; red) are aligned on a line spanning $L/4$. After travelling for a distance $L/2$, the fishing agent array is recreated at a distance of $L/4$ away from the center of mass of the shoal and restarts its movement in its direction.

Results

A. Shoaling behavior.

We found a significant effect of the selection lines on mean inter-individual independently on

DRAFT

measuring it in cm ($\chi^2_{(2)} = 8.8$; $p < 0.05$) or mean body length ($\chi^2_{(2)} = 7.4$; $p < 0.05$; Fig. 3A). By contrast, we found a trend of selection lines on mean nearest-neighbor distance when measuring it in cm ($\chi^2_{(2)} = 5.3$; $p = 0.070$; Fig. 3A), while it had a significant effect when measuring it in body length ($\chi^2_{(2)} = 7.8$; $p < 0.05$; Fig. 3A). In particular, the large- and small-harvested lines tend to form less and more cohesive shoals than controls, respectively (Fig. 3A). Moreover, we did not find a significant effect of selection lines on group polarization ($\chi^2_{(2)} = 0.7$; $p = 0.716$; mean and standard deviation across selection lines: 0.40 ± 0.06). We also found a negative correlation (Rc = -0.38 ; $F_{(1,28)}$= 12.5; $p <$ 0.01) between mean nearest-neighbor distance and the previously documented risk-taking behavior (Fig. 3B; note that in this study we used the same groups of fish previously used to test risk-taking behavior, see methods for more details). Furthermore, the inter-individual distance and the nearest-neighbor distance also showed a strong positive correlation (Rc = 0.88; $F_{(1,28)}$= 207.2; p < 0.001), which means that the change in inter-individual distance was not related to a split of the main group into multiple subgroups.

B. Fish body size and individual behavior in the shoal. As expected, the body size at age of the experimental fish varied significantly among the selection lines ($\chi^2_{(2)} = 28.3$; $p <$ 0.001; Fig. 3C). The individual burst rate within the shoal was significantly ($\chi^2_{(2)} = 44.6$; $p < 0.001$) different among selection lines. Specifically, the small-, but not the large-harvested line, bursted less frequently than controls (Fig. 3D). Furthermore, the individual swimming speed was significantly ($\chi^2_{(2)} = 47.8$; $p < 0.001$) different among selection lines. Again, the small-, but not the large-harvested line, showed a slower swimming speed than controls (Fig. 3E). Note that the burst rate showed a positive correlation with the swimming speed (R = 0.51; $F_{(1,142)}$= 148.6; p < 0.001; Fig. 3F), which suggests that differences in burst rate was the main cause of variation in swimming speed.

To control possible confounding effects of body size on the effects of size-selective harvesting on behavior (see methods for more details) we composed a subsample of the dataset with size-matched individuals without significant ($\chi^2_{(2)} =$ 1.1; $p = 0.592$) differences in body length among the lines (Fig. 3C). The above mentioned differences in speed and burst rate among the selection lines were still significant for both burst rate ($\chi^2_{(2)} = 34.1$; $p < 0.001$; Fig. 3D) and speed ($\chi^2_{(2)} = 32.6$; $p < 0.001$; Fig. 3E) when the subsample of size-matched individuals was used in the analyses. Moreover, body size did not relate to burst rate ($\chi^2_{(2)} = 0.03$; $p = 0.858$) and swimming speed ($\chi^2_{(2)} = 0.4$; $p = 0.519$).

C. Mechanistically linking micro-level interactions among individuals with macro-level collective outcomes. We allowed each parameter except of the friction coefficient to vary between the model representations of the selection lines (parameters summarized in Tab. S1). The selection lines were about equal in burst duration (t_b) and the

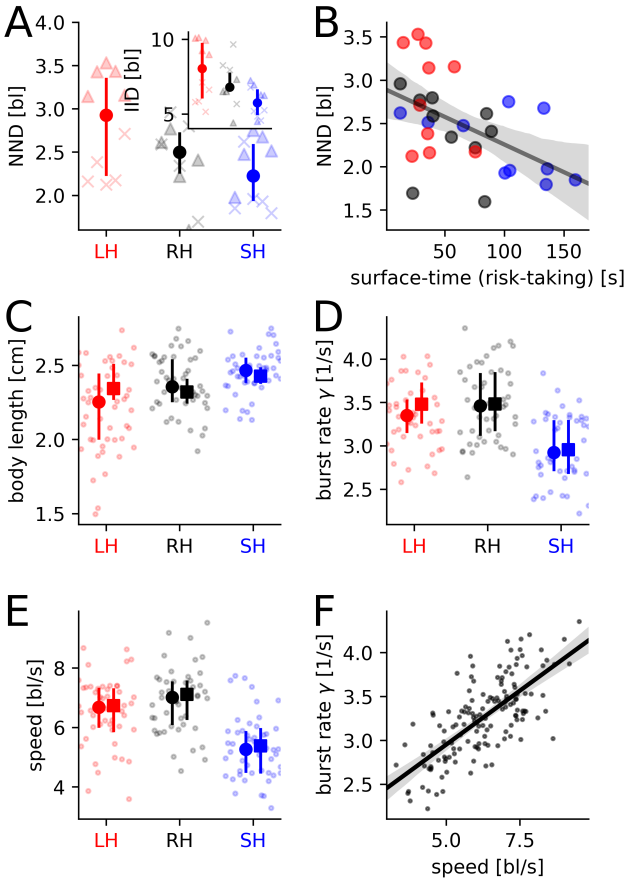

Fig. 3. Group level results for mean nearest-neighbor distance (in body length; **A**) and inter-individual distance (in body length; inset **A**) together with the correlation between mean nearest-neighbor distance and previously documented risk-taking behavior (i.e. time spent feeding at the surface, **B**; see (42) for more details; note that in this study we used the same groups of fish previously used to test risk-taking behavior, see methods for more details). Individual level results for body size (**C**), burst rate (**D**), and speed (expressed in body length per second; **E**) according to high resolution tracking (30 frames per second), as well as the correlation between burst rate and speed (**F**). The selection lines are indicated by different colors (red=LH: large-harvested; black=RH: random-harvested; blue=SH: small-harvested). Bold vertical lines with circles (**C-E**) refer to the entire data set (N = 48), while bold lines with squares refer to the subsample of size-matched individuals (N = LH: 24; RH: 36; SH: 40). The bold circle and square represent the median and vertical lines represent the first (25th percentile) and third (75th percentile) quartiles. Triangles and crosses (**A**) correspond to raw data of the two different replicates.

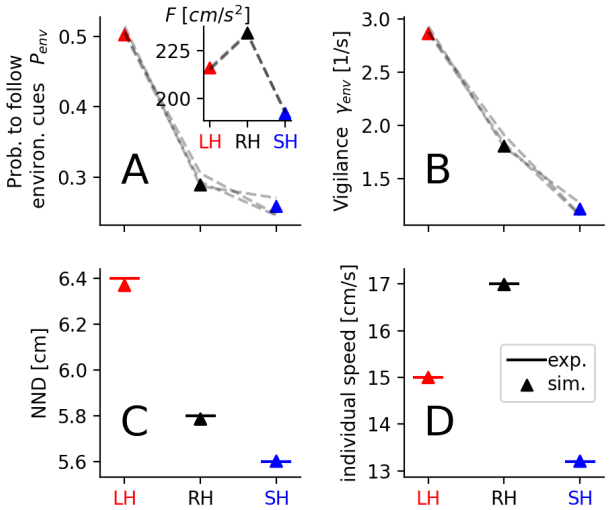

Fig. 4. Fitted model representation of the different selection lines. In order to resemble the experimental observations the probability to follow environmental cues (**A**) and the burst force (inset **A**) were set for each selection line. The vigilance γ_{env} is the product of P_{env} and the burst rate γ (**B**). The average nearest neighbor distance (NND, **C**) and the average individual speed (**D**) are emergent properties of the model and were used to quantify how well the parameters (P_{env}, γ) reproduce the experimental observations. Triangles represent the model parameters or the simulation outcomes of the parameter set with the best match to the experiment. Dashed lines (**A, B**) represent a parameter set of a different initialization, and therefore show the robustness of the best matching parameter set (triangles). The horizontal solid lines (**C, D**) represent the experimental values. Note that in contrast to Fig. 3 units are in cm because the modelled agents have no body length. The selection lines are indicated by different colors (red=LH: large-harvested; black=RH: random-harvested; blue=SH: small-harvested).

differences in burst rate (γ) corresponded qualitatively to the experimental equivalents (Fig. 3D). The range of the social zones (r_r, r_o, r_a) differed in the same manner as the experimentally observed body lengths (Fig. 3C), i.e. the in average smaller fish (LH line) have a shorter repulsion, orientation and attraction zone and vice verse for the larger fish (SH line). The probability to follow environmental cues (P_{env}, Fig. 4A) and the burst force (F, inset Fig. 4A) were set such that the model representations of nearest neighbor distance (Fig. 4C) and mean individual speed (Fig. 4D) were as close as possible to the experimental data. Interestingly, the closely related vigilance (product of burst rate and P_{env}) was for the large-harvested line greater than control, and vice versa for the small-harvested line (Fig. 4B). The same qualitative differences were reported for the risk taking behavior in a previous study (42). Therefore, a possible mechanistic explanation for the observed differences in cohesion is that the more risk-taking individuals of the small-harvested line were less vigilant, which causes them to respond less frequently to environmental cues, instead of social cues, which consequently increased their cohesion (vice versa for the large-harvested line). To substantiate this explanation we re-estimated the parameters F, P_{env} by enforcing that all selection line shared the same P_{env}. Without the ability to differ in P_{env}, and thus in vigilance, the model representations were unable to reproduce the experimentally observed cohesion pattern (Fig. S12).

D. Exploitation rates in the predator and fishing context. The simulation results show that if the natural predator moved slow, both size-selected lines had a higher exploitation rate than controls (Fig. 5C). By contrast, when the predator moved faster, the large-harvested line was more efficiently exploited than the controls, while the small-harvested line did not showed major differences. In both fishing scenarios (Fig. 5D, E), the large-harvested had a lower exploitation rate than the control, and vice versa for the small-harvested line (Fig. 5D, E). Please note that when the confusion effect is turned off, the exploitation rates observed in the natural predator scenarios are similar to those of the fishing scenarios (Fig. S3B). It suggests that the differences in group cohesion among the selection lines (Fig. 4C) influence the exploitation rate of the natural predator (i.e., confusion effect is stronger in more cohesive shoals). The confusion effect as explanation is further supported by the average distance of the shoaling fish from the predator/fishing agent. The distance was greater than control in all the scenario for the large harvested line, and vice verse for the small harvested line (Fig. S3 I-P). Thus, the fish shoals avoid the natural predator as good as they avoid the fishing agents but the predator gets confused according to their respective cohesion (for details see Sect. III).

Discussion

We showed that five generations of size-selective mortality followed by eight generations during which harvesting halted left a legacy in terms of collective behaviour. Shoal cohesion changed in the opposite direction to what was expected considering previous studies on the same experimental system. In particular, we documented that shoal cohesion was negatively correlated with previously documented group risk-taking behaviour (Fig. 3B). Therefore, our experimental hypothesis was rejected and unexpected results discussed in terms of possible direct selection on sociability. Moreover, by using the agent-based model implemented here we proposed a possible explanation that links group risk-taking behaviour to individual vigilance and consequently to shoal cohesion. Finally, the simulations of fishing scenarios suggested that the collective behavioural changes induced by large size-selective mortality (i.e., a typical selectivity pattern in many fisheries) may be adaptive in a fishing scenario, but maladaptive with respect to natural predation.

The changes of shoal cohesion we documented may be interpreted in light of a behavioural-mediated resource acquisition mechanism that affected size-at-harvest as trait under selection (42, 59). Zebrafish can attain a higher food consumption rate when they are in small groups than alone (60). Therefore, the large size-selective mortality treatment could have removed bolder individuals that fed in small groups because such behaviour could have provided advantages in accessing food and hence increased size-at-harvest; this could have fostered the evolution of reduced shoal cohesion (and vice versa for the small size-selective mortality). However, previous results on the selection lines showed that when assaying indi-

DRAFT

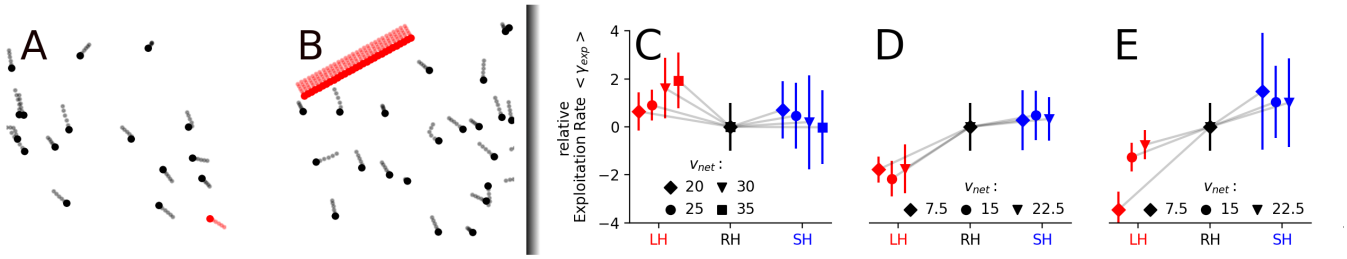

Fig. 5. Simulation snapshots are shown for the predator- and single-fishing-agent scenario (**A**) and for the multiple-fishing-agents scenario (**B**); with shoaling fish in black and the predator and fishing agents in red. The exploitation rate, i.e. prey captured per time unit, was computed for a natural predator moving with $v_{net} = [20,\ 25,\ ,30,\ 35]\ cm/s$ (**C**); for a single fishing agent (**D**) and for multiple fishing agents distributed on a line (**E**). The fishing agents moved with $v_{net} = [7.5,\ 15,\ 22.5]\ cm/s$ indicated by rhombus, circle and triangle, respectively. The shoaling fish had a mean speed of about $\langle v \rangle \approx 15\ cm/s$. The markers (**C, D, E**) represent the relative exploitation rates, i.e. the exploitation rates were reduced by the mean and divided by the standard deviation of the random-harvested line. The markers and error bars indicate the mean and standard deviation estimated from samples of 400 simulations of $N = 30$ shoaling fish in a box of size $L = 100\ cm$ with periodic boundary conditions. The colors red, black and blue correspond to the large- (LH), random- (RH) and small-harvested (SH) selection line, respectively.

vidual female sociability, the small-harvested line was found to be less social than control, while the large-harvested line was not found to differ from controls (40). Thus, we suggested that direct selection on sociability was not a major driver of the changes in shoal cohesion documented here, rather we propose an explanation based on a mechanistic process that emerged from the agent-based model calibration.

The burst-coast-agent-based model linked risk-taking behaviour with shoal cohesion and further helped explaining the harvesting-induced changes in collective behaviour by assuming the existence of a trade-off between social and environmental information in collective motion (61). Our model is similar to previous work in terms of splitting the movement of shoaling fish into an active and passive phase (19, 62, 63). However, it provides a novel perspective about collective movements of fish shoals by linking risk perception and movement decisions. In fact, most previous models of collective behaviour only accounted for social information (19, 22, 62, 64, 65), while our model explicitly implements the trade-off between random environmental and social cues. The previous simulation studies which considered similar mechanisms (e.g., when moving agents directly react to a non-conspecific cue as a predator (66, 67) or a food-patch (68)) allowed the moving agents to access non-social information without a permanent cost, i.e. the trade-off only exists with a present environmental cue. In our model, the vigilance limits the general capacity to react to social cues and thus affects the individual behaviour even in the absence of environmental cues. Another major difference to most existing models (19, 22, 28, 65) is that the individual speed is not a model parameter but emerges from the interplay of burst rate, strength, duration and the tendency to follow environmental cues. Especially, accounting for the possibility of individual burst being triggered by either social or environmental cues adds a novel, yet ecologically relevant behavioural dimension to our agent-based model.

The simulations of natural predation and fishing revealed that the collective behavioral changes of the large-harvested line are likely adaptive in a fishing context, but maladaptive under natural predation. Specifically, in our simulations the increase in vigilance of the large-harvested line decreased vulnerability of shoals under a multitude of simulated fishing scenarios considering single and multiple fishing agents moving at different speed. Fisheries-induced evolution of maladaptive collective behavioral traits (i.e. shoal cohesion) can have strong repercussions in many shoaling teleosts when attempting to reduce risk of natural predation (16). Our study suggests that intensive fishing mortality directed at the larger individuals of a population could shift the fitness optimum of shoaling behavior in the opposite direction of what natural selection would favor. Evolution under anthropogenic selection has been demonstrated to occur within few generations (3, 7, 39, 69–71), and could impede recovery of exploited population even after harvesting halted (72). This is the first functional integration of individual vigilance into mechanisms governing group dynamics with respect to fisheries exploitation and natural predation. An alternative mechanism, recently proposed by Guerra et al. (38), is purely based on group size, which is expected to decrease in response to fishing exploitation and subsequently decrease fitness in response to natural predation. Therefore, it is plausible that fisheries-induced evolution affect multiple traits related to shoaling behavior that could vary depending from the specific fishing gear used and the ecology of the exploited species (23). Our work proposes a new mechanism that could increase the natural mortality associated with fisheries-induced evolution and thereby negatively affect recovery, even if harvesting halted.

Previous studies have shown that fisheries-induced evolution of life histories can substantially increase natural mortality (10, 73). Elevated and size-selective harvesting triggers the evolution of a fast life-history, characterized by early maturation and small size, elevated reproductive investment and reduced post-maturation growth (74). Natural mortality decreases with length in fishes (2); therefore a decrease in body size is linked to an increase in natural mortality. In addition, an increase in reproductive investment is associated to an increase in natural mortality due to the cost of spawning (10, 75). Moreover, elevated and unselective fishing mortality is expected to increase risk-taking behavior, which in turn increases natural mortality (10). Previous experimental results using the zebrafish selection lines indicated that elevated mortality in combination with large size-selective harvest decreased collective risk-taking behavior (42), which

DRAFT

agrees with recent theoretical work (6). Yet, while decreased risk-taking might reduce natural mortality, we propose that the decrease in shoal cohesion emerging from the evolution of decreased risk-taking behavior can be a further mechanism by which natural mortality increases in a fisheries-induced evolution context where large individuals are preferentially harvested. We therefore extended the framework presented by Jørgensen and Holt (10) for unselective fisheries harvest revealing an insofar unknown mechanism by which fisheries-induced evolution of individual behavioral trait (e.g. risk-taking behavior) through size-selection may drive collective outcomes that may be maladaptive under natural predation and elevate mortality in shoaling fishes. This is particularly important in an ecosystem context where trophic flow between predator and prey is controlled by a bottom-up mechanism mediated by prey behavior (76).

Conclusions and implications

Our study suggests that size-selective mortality can alter the collective behavior of fishes. The harvesting-induced behavioral changes that are adaptive under a fishing scenario can produce a maladaptive response in a natural predation context. One limitation of our work is that our experimental approach lacks natural predators. Therefore, the transfer of our research into the wild is limited, and more studies in real fisheries contexts are needed. If the results hold in the wild, however, they would have substantial consequences for global fisheries by increasing natural mortality rates of exploited shoaling species. The harvesting-induced changes we documented may slowly, but steadily erode the natural adaptive value of shoaling behavior in many species targeted by global fisheries.

Data and codes availability. Experimental data are available as supplementary material together with the R code used for statistical analysis. The code to run the burst and coast model with the fishing/predator scenarios is available at github (`https://github.com/PaPeK/sde_burst_coast`). The optimization was done with a python implementation of the CMA-ES (`https://github.com/CMA-ES/pycma`).

Competing interests. The authors declare no competing interests

Bibliography

1. Susan M Sogard. Size-selective mortality in the juvenile stage of teleost fishes: a review. *Bulletin of marine science*, 60(3):1129–1157, 1997. ISSN 0007-4977.
2. Kai Lorenzen. Allometry of natural mortality as a basis for assessing optimal release size in fish-stocking programmes. *Canadian Journal of Fisheries and Aquatic Sciences*, 57(12): 2374–2381, 2000. ISSN 0706-652X. doi: 10.1139/f00-215.
3. Mikko Heino, Beatriz Díaz Pauli, and Ulf Dieckmann. Fisheries-induced evolution. *Annual Review of Ecology, Evolution and Systematics*, 46(1):461–480, 2015. ISSN 1543-592X. doi: 10.1146/annurev-ecolsys-112414-054339.
4. Daniele D'Agostino, Carlos Jimenez, Tom Reader, Louis Hadjioannou, Stephanie Heyworth, Marilena Aplikioti, Marina Argyrou, and David A. Feary. Behavioural traits and feeding ecology of mediterranean lionfish and native species naiveté to lionfish predation. *bioRxiv*, page 2020.01.22.915322, 2020. doi: 10.1101/2020.01.22.915322.
5. Anssi Karvonen, Päivi Rintamäki, Jukka Jokela, and E. Tellervo Valtonen. Increasing water temperature and disease risks in aquatic systems: Climate change increases the risk of some, but not all, diseases. *International Journal for Parasitology*, 40(13):1483–1488, 2010. ISSN 0020-7519. doi: https://doi.org/10.1016/j.ijpara.2010.04.015.
6. Ken H. Andersen, Lise Marty, and Robert Arlinghaus. Evolution of boldness and life history in response to selective harvesting. *Canadian Journal of Fisheries and Aquatic Sciences*, 75(2):271–281, 2018. ISSN 0706-652X 1205-7533. doi: 10.1139/cjfas-2016-0350.
7. David O. Conover and Stephan B. Munch. Sustaining fisheries yields over evolutionary time scales. *Science*, 297(5578):94–96, 2002. doi: 10.1126/science.1074085.
8. J. Hollins, D. Thambithurai, B. Koeck, A. Crespel, D. M. Bailey, S. J. Cooke, J. Lindstrom, K. J. Parsons, and S. S. Killen. A physiological perspective on fisheries-induced evolution. *Evolutionary Applications*, 11(5):561–576, 2018. ISSN 1752-4571 (Print) 1752-4571 (Linking). doi: 10.1111/eva.12597.
9. Steven Brady, Daniel I. Bolnick, Rowan D. H. Barrett, Lauren J. Chapman, Erika Crispo, Alison M. Derry, Christopher G. Eckert, Dylan J. Fraser, Gregor F. Fussmann, Andrew Gonzalez, Frédéric Guichard, Thomas Lamy, Jeffrey E. Lane, Andrew G. McAdam, Amy E. M. Newman, Antoine Paccard, Bruce Robertson, Gregor Rolshausen, Patricia M. Schulte, Andrew M. Simons, Mark Vellend, and Andrew P. Hendry. Understanding maladaptation by uniting ecological and evolutionary perspectives. *The American Naturalist*, 2019. ISSN 0003-0147. doi: 10.1086/705020.
10. Christian Jørgensen and Rebecca E. Holt. Natural mortality: Its ecology, how it shapes fish life histories, and why it may be increased by fishing. *Journal of Sea Research*, 75:8–18, 2013. ISSN 1385-1101. doi: http://dx.doi.org/10.1016/j.seares.2012.04.003.
11. Andrew Sih, Maud C. O. Ferrari, and David J. Harris. Evolution and behavioural responses to human-induced rapid environmental change. *Evolutionary Applications*, 4(2):367–387, 2011. ISSN 1752-4571. doi: 10.1111/j.1752-4571.2010.00166.x.
12. Ulla Tuomainen and Ulrika Candolin. Behavioural responses to human-induced environmental change. *Biological Reviews*, 86(3):640–657, 2011. ISSN 1464-7931.
13. Bob B.M. Wong and Ulrika Candolin. Behavioral responses to changing environments. *Behavioral Ecology*, 26(3):665–673, 2014. ISSN 1045-2249. doi: 10.1093/beheco/aru183.
14. W. D. Hamilton. Geometry for the selfish herd. *Journal of Theoretical Biology*, 31(2):295–311, 1971. ISSN 0022-5193. doi: https://doi.org/10.1016/0022-5193(71)90189-5.
15. Jens Krause and Graeme D Ruxton. *Living in groups*. Oxford University Press, 2002. ISBN 0198508182.
16. TJ Pitcher, AE Magurran, and IJ Winfield. Fish in larger shoals find food faster. *Behavioral Ecology and Sociobiology*, 10(2):149–151, 1982. ISSN 0340-5443.
17. Julia K. Parrish. Using behavior and ecology to exploit schooling fishes. *Environmental Biology of Fishes*, 55(1):157–181, 1999. ISSN 1573-5133. doi: 10.1023/A:1007472602017.
18. Alexander Kotrschal, Alexander Szorkovszky, James Herbert-Read, Natasha I. Bloch, Maksym Romenskyy, Séverine Denise Buechel, Ada Fontrodona Eslava, Laura Sánchez Alòs, Hongli Zeng, Audrey Le Foll, Ganaël Braux, Kristiaan Pelckmans, Judith E. Mank, David Sumpter, and Niclas Kolm. Rapid evolution of coordinated and collective movement in response to artificial selection. *bioRxiv*, page 2020.01.30.926311, 2020. doi: 10.1101/2020.01.30.926311.
19. Daniel S. Calovi, Alexandra Litchinko, Valentin Lecheval, Ugo Lopez, Alfonso Pérez Escudero, Hugues Chaté, Clément Sire, and Guy Theraulaz. Disentangling and modeling interactions in fish with burst-and-coast swimming reveal distinct alignment and attraction behaviors. *PLOS Computational Biology*, 14(1):e1005933, jan 2018. ISSN 1553-7358. doi: 10.1371/journal.pcbi.1005933.
20. Iain D. Couzin and Jens Krause. *Self-Organization and Collective Behavior in Vertebrates*, volume 32, pages 1–75. Academic Press, 2003. ISBN 0065-3454. doi: https://doi.org/10.1016/S0065-3454(03)01001-5.
21. James E Herbert-Read, Andrea Perna, Richard P Mann, Timothy M Schaerf, David JT Sumpter, and Ashley JW Ward. Inferring the rules of interaction of shoaling fish. *Proceedings of the National Academy of Sciences, USA*, 108(46):18726–18731, 2011. ISSN 0027-8424.
22. Iain D Couzin, Jens Krause, Richard James, Graeme D Ruxton, and Nigel R Franks. Collective memory and spatial sorting in animal groups. *Journal Theoretical Biology*, 218(1): 1–11, 2002. ISSN 00225193. doi: 10.1006/yjtbi.3065.
23. Marion Claireaux, Christian Jørgensen, and Katja Enberg. Evolutionary effects of fishing gear on foraging behavior and life-history traits. *Ecology and Evolution*, 8(22):10711–10721, 2018. ISSN 2045-7758 (Print) 2045-7758 (Linking). doi: 10.1002/ece3.4482.
24. Robert Arlinghaus, Kate L. Laskowski, Josep Alós, Thomas Klefoth, Christopher T. Monk, Shinnosuke Nakayama, and Arne Schröder. Passive gear-induced timidity syndrome in wild fish populations and its potential ecological and managerial implications. *Fish and Fisheries*, 18(2):360–373, 2017. ISSN 1467-2979. doi: 10.1111/faf.12176.
25. Silva Uusi-Heikkilä, Christian Wolter, Thomas Klefoth, and Robert Arlinghaus. A behavioral perspective on fishing-induced evolution. *Trends in Ecology & Evolution*, 23(8):419–421, 2008. ISSN 0169-5347. doi: 10.1016/j.tree.2008.04.006.
26. Jolle W. Jolles, Andrew J. King, and Shaun S. Killen. The role of individual heterogeneity in collective animal behaviour. *Trends in Ecology & Evolution*, 35(3):278–291, 2020. ISSN 0169-5347. doi: https://doi.org/10.1016/j.tree.2019.11.001.
27. Zhong-Hua Tang and Shi-Jian Fu. Qingbo (*Spinibarbus sinensis*) personalities and their effect on shoaling behavior. *Acta Ethologica*, 22(2):135–144, 2019. ISSN 0873-9749.
28. Jolle W Jolles, Neeltje J Boogert, Vivek H Sridhar, Iain D Couzin, and Andrea Manica. Consistent individual differences drive collective behavior and group functioning of schooling fish. *Current Biology*, 27(18):2862–2868, 2017. ISSN 0960-9822.
29. Kolbjørn Tunstrøm, Yael Katz, Christos C. Ioannou, Cristián Huepe, Matthew J. Lutz, and Iain D. Couzin. Collective states, multistability and transitional behavior in schooling fish. *PLOS Computational Biology*, 9(2):e1002915, 2013. doi: 10.1371/journal.pcbi.1002915.
30. Hannah E. A. MacGregor, James E. Herbert-Read, and Christos C. Ioannou. Information can explain the dynamics of group order in animal collective behaviour. *Nature Communications*, 11(1):2737, dec 2020. ISSN 2041-1723. doi: 10.1038/s41467-020-16578-x.
31. P. Domenici and R. S. Batty. Escape behaviour of solitary herring (Clupea harengus) and comparisons with schooling individuals. *Marine Biology*, 128(1):29–38, apr 1997. ISSN 0025-3162. doi: 10.1007/s002270050065.
32. Guy Beauchamp. Group-size effects on vigilance: A search for mechanisms. *Behavioural Processes*, 63(3):111–121, 2003. ISSN 03766357. doi: 10.1016/S0376-6357(03)00002-0.
33. Guy Beauchamp. What is the magnitude of the group-size effect on vigilance? *Behavioral Ecology*, 19(6):1361–1368, 2008. ISSN 10452249. doi: 10.1093/beheco/arn096.
34. Ashley J.W. Ward, James E. Herbert-Read, David J.T. Sumpter, and Jens Krause. Fast and accurate decisions through collective vigilance in fish shoals. *Proceedings of the National Academy of Sciences of the United States of America*, 108(6):2312–2315, 2011. ISSN 10916490. doi: 10.1073/pnas.1007102108.
35. Sybille Hess, Stefan Fischer, and Barbara Taborsky. Territorial aggression reduces vigi-

DRAFT

lance but increases aggression towards predators in a cooperatively breeding fish. *Animal Behaviour*, 113:229–235, 2016. ISSN 00033472. doi: 10.1016/j.anbehav.2016.01.008.

36. A. M. Edwards, E. C. Best, S. P. Blomberg, and A. W. Goldizen. Individual traits influence vigilance in wild female eastern grey kangaroos. *Australian Journal of Zoology*, 61(4):332–341, 2013. ISSN 0004959X. doi: 10.1071/ZO13025.
37. Kenta Uchida, Kei K. Suzuki, Tatsuki Shimamoto, Hisashi Yanagawa, and Itsuro Koizumi. Decreased vigilance or habituation to humans? Mechanisms on increased boldness in urban animals. *Behavioral Ecology*, 30(6):1583–1590, 2019. ISSN 14657279. doi: 10.1093/beheco/arz117.
38. Ana Sofia Guerra, Albert B Kao, Douglas J McCauley, and Andrew M Berdahl. Fisheries-induced selection against schooling behaviour in marine fishes. *Proc. R. Soc. B Biol. Sci.*, 287(1935):20201752, sep 2020. ISSN 0962-8452. doi: 10.1098/rspb.2020.1752.
39. Silva Uusi-Heikkilä, Andrew R. Whiteley, Anna Kuparinen, Shuichi Matsumura, Paul A. Venturelli, Christian Wolter, Jon Slate, Craig R. Primmer, Thomas Meinelt, Shaun S. Killen, David Bierbach, Giovanni Polverino, Arne Ludwig, and Robert Arlinghaus. The evolutionary legacy of size-selective harvesting extends from genes to populations. *Evolutionary Applications*, 8(6):597–620, 2015. ISSN 1752-4571. doi: 10.1111/eva.12268.
40. Valerio Sbragaglia, Josep Alós, Kim Fromm, Christopher T. Monk, Carlos Díaz-Gil, Silva Uusi-Heikkilä, Andrew E. Honsey, Alexander D.M. Wilson, and Robert Arlinghaus. Experimental size-selective harvesting affects behavioral types of a social fish. *Transactions of the American Fisheries Society*, 148(3):552–568, 2019. ISSN 0002-8487 1548-8659. doi: 10.1002/tafs.10160.
41. V. Sbragaglia, C. Gliese, D. Bierbach, A. E. Honsey, S. Uusi-Heikkila, and R. Arlinghaus. Size-selective harvesting fosters adaptations in mating behaviour and reproductive allocation, affecting sexual selection in fish. *Journal of Animal Ecology*, 88(9):1343–1354, 2019. ISSN 0021-8790. doi: 10.1111/1365-2656.13032.
42. Valerio Sbragaglia, Jose Fernando López-Olmeda, Elena Frigato, Cristiano Bertolucci, and Robert Arlinghaus. Fisheries-induced evolution of the circadian system and collective personality traits. *bioRxiv*, page 622043, 2019. doi: 10.1101/622043.
43. Silva Uusi-Heikkilä, Kai Lindström, Noora Parre, Robert Arlinghaus, Josep Alós, and Anna Kuparinen. Altered trait variability in response to size-selective mortality. *Biology Letters*, 12(9):20160584, 2016. doi: 10.1098/rsbl.2016.0584.
44. S. Uusi-Heikkilä, T. Savilammi, E. Leder, R. Arlinghaus, and C. R. Primmer. Rapid, broad-scale gene expression evolution in experimentally harvested fish populations. *Molecular Ecology*, 26(15):3954–3967, 2017. ISSN 1365-294X (Electronic) 0962-1083 (Linking). doi: 10.1111/mec.14179.
45. Allan V Kalueff. *The rights and wrongs of zebrafish: Behavioral phenotyping of zebrafish*. Springer International Publishing Switzerland, 2017.
46. N. Speedie and R. Gerlai. Alarm substance induced behavioral responses in zebrafish (*Danio rerio*). *Behav Brain Res*, 188(1):168–77, 2008. ISSN 0166-4328 (Print) 0166-4328. doi: 10.1016/j.bbr.2007.10.031.
47. S. Uusi-Heikkilä, C. Wolter, T. Meinelt, and R. Arlinghaus. Size-dependent reproductive success of wild zebrafish *Danio rerio* in the laboratory. *Journal of Fish Biology*, 77(3):552–69, 2010. ISSN 0022-1112. doi: 10.1111/j.1095-8649.2010.02698.x.
48. K. O. Darrow and W. A. Harris. Characterization and development of courtship in zebrafish, *Danio rerio. Zebrafish*, 1(1):40–5, 2004. ISSN 1545-8547. doi: 10.1089/154585404774101662.
49. Alfonso Pérez-Escudero, Julián Vicente-Page, Robert C. Hinz, Sara Arganda, and Gonzalo G. de Polavieja. idtracker: tracking individuals in a group by automatic identification of unmarked animals. *Nature Methods*, 11(7):743–748, 2014. doi: 10.1038/nmeth.2994https://www.nature.com/articles/nmeth.2994#supplementary-information.
50. G. Polverino, D. Bierbach, S. S. Killen, S. Uusi-Heikkila, and R. Arlinghaus. Body length rather than routine metabolic rate and body condition correlates with activity and risk-taking in juvenile zebrafish *Danio rerio*. *Journal of Fish Biology*, 89(5):2251–2267, 2016. ISSN 0022-1112. doi: 10.1111/jfb.13100.
51. Pawel Romanczuk, Markus Bär, Werner Ebeling, Benjamin Lindner, and Lutz Schimansky-Geier. Active brownian particles. *The European Physical Journal Special Topics*, 202(1):1–162, 2012.
52. Ariana Strandburg-Peshkin, Colin R. Twomey, Nikolai W F Bode, Albert B. Kao, Yael Katz, Christos C. Ioannou, Sara B. Rosenthal, Colin J. Torney, Hai Shan Wu, Simon A. Levin, and Iain D. Couzin. Visual sensory networks and effective information transfer in animal groups. *Current Biology*, 23(17):R709–R711, 2013. ISSN 09609822. doi: 10.1016/j.cub.2013.07.059.
53. Nikolaus Hansen and Andreas Ostermeier. Adapting arbitrary normal mutation distributions in evolution strategies: The covariance matrix adaptation. *Proceedings of IEEE International Conference on Evolutionary Computation*, pages 312–317, 1996. doi: 10.1109/ICEC.1996.542381.
54. Nikolaus Hansen, Youhei Akimoto, and Petr Baudis. Cma-es/pycma on github. Zenodo, DOI:10.5281/zenodo.2559634, 2019.
55. Manfred Milinski. Experiments on the selection by predators against spatial oddity of their prey. *Zeitschrift für Tierpsychologie*, 43(3):311–325, 1977. ISSN 0044-3573. doi: 10.1111/j.1439-0310.1977.tb00078.x.
56. Paolo Domenici. The scaling of locomotor performance in predator–prey encounters: from fish to killer whales. *Comparative Biochemistry and Physiology Part A: Molecular & Integrative Physiology*, 131(1):169–182, 2001. ISSN 1095-6433. doi: https://doi.org/10.1016/S1095-6433(01)00465-2.
57. Howard C Howland. Optimal strategies for predator avoidance: the relative importance of speed and manoeuvrability. *Journal of Theoretical Biology*, 47(2):333–350, 1974. ISSN 0022-5193.
58. Laurie Landeau and John Terborgh. Oddity and the 'confusion effect'in predation. *Animal Behaviour*, 34(5):1372–1380, 1986. ISSN 0003-3472.
59. Katja Enberg, Christian Jørgensen, Erin S. Dunlop, Øystein Varpe, David S. Boukal, Loïc Baulier, Sigrunn Eliassen, and Mikko Heino. Fishing-induced evolution of growth: concepts, mechanisms and the empirical evidence. *Marine Ecology*, 33(1):1–25, 2012. ISSN 1439-0485. doi: 10.1111/j.1439-0485.2011.00460.x.
60. Roy Harpaz and Elad Schneidman. Social interactions drive efficient foraging and income equality in groups of fish. *bioRxiv*, page 740886, 2019. doi: 10.1101/740886.
61. Parisa Rahmani, Fernando Peruani, and Pawel Romanczuk. Flocking in complex environments—attention trade-offs in collective information processing. *PLOS Computational Biology*, 16(4):e1007697, 2020. doi: 10.1371/journal.pcbi.1007697.
62. Nikolai W.F. Bode, Jolyon J. Faria, Daniel W. Franks, Jens Krause, and A. Jamie Wood. How perceived threat increases synchronization in collectively moving animal groups. *Proceedings of the Royal Society B: Biological Sciences*, 277(1697):3065–3070, 2010. ISSN 14712970. doi: 10.1098/rspb.2010.0855.
63. Roy Harpaz, Gašper Tkačik, and Elad Schneidman. Discrete modes of social information processing predict individual behavior of fish in a group. *Proceedings of the National Academy of Sciences, USA*, 114(38):10149–10154, 2017. ISSN 1091-6490 0027-8424. doi: 10.1073/pnas.1703817114.
64. Pawel Romanczuk, Iain D. Couzin, and Lutz Schimansky-Geier. Collective motion due to individual escape and pursuit response. *Physical Review Letters*, 102(1):010602, jan 2009. ISSN 0031-9007. doi: 10.1103/PhysRevLett.102.010602.
65. Tamás Vicsek, András Czirók, Eshel Ben-Jacob, Inon Cohen, and Ofer Shochet. Novel type of phase transition in a system of self-driven particles. *Physical Review Letters*, 75(6):1226–1229, aug 1995. ISSN 0031-9007. doi: 10.1103/PhysRevLett.75.1226.
66. Jure Demšar, Charlotte K. Hemelrijk, Hanno Hildenbrandt, and Iztok Lebar Bajec. Simulating predator attacks on schools: Evolving composite tactics. *Ecological Modelling*, 304:22–33, may 2015. ISSN 03043800. doi: 10.1016/j.ecolmodel.2015.02.018.
67. Randal S. Olson, David B. Knoester, and Christoph Adami. Evolution of swarming behavior is shaped by how predators attack. *Artificial Life*, 22(3):299–318, 2016. doi: 10.1162/ARTL_a_00206%M27139941.
68. Iain D. Couzin, Jens Krause, Nigel R Franks, and Simon A. Levin. Effective leadership and decision making in animal groups on the move. *Nature*, 13(4):513–516, 2005. ISSN 14607425. doi: 10.1038/nature03236.
69. Stephanie M. Carlson, Curry J. Cunningham, and Peter A. H. Westley. Evolutionary rescue in a changing world. *Trends in Ecology & Evolution*, 29(9):521–530, 2014. ISSN 0169-5347. doi: https://doi.org/10.1016/j.tree.2014.06.005.
70. Clémentine Renneville, Alexis Millot, Simon Agostini, David Carmignac, Gersende Maugars, Sylvie Dufour, Arnaud Le Rouzic, and Eric Edeline. Anthropogenic selection along directions of most evolutionary resistance. *bioRxiv*, page 498683, 2018. doi: 10.1101/498683.
71. Serinde J. van Wijk, Martin I. Taylor, Simon Creer, Christine Dreyer, Fernanda M. Rodrigues, Indar W. Ramnarine, Cock van Oosterhout, and Gary R. Carvalho. Experimental harvesting of fish populations drives genetically based shifts in body size and maturation. *Frontiers in Ecology and the Environment*, 11(4):181–187, 2013. ISSN 1540-9309. doi: 10.1890/120229.
72. Katja Enberg, Christian Jørgensen, Erin S. Dunlop, Mikko Heino, and Ulf Dieckmann. Implications of fisheries-induced evolution for stock rebuilding and recovery. *Evolutionary Applications*, 2(3):394–414, 2009. ISSN 1752-4571. doi: 10.1111/j.1752-4571.2009.00077.x.
73. Christian Jørgensen and Oyvind Fiksen. Modelling fishing-induced adaptations and consequences for natural mortality. *Canadian Journal of Fisheries and Aquatic Sciences*, 67(7):1086–1097, 2010. ISSN 0706-652X. doi: 10.1139/F10-049.
74. Diana M. T. Sharpe and Andrew P. Hendry. Life history change in commercially exploited fish stocks: an analysis of trends across studies. *Evolutionary Applications*, 2(3):260–275, 2009. ISSN 1752-4571. doi: 10.1111/j.1752-4571.2009.00080.x.
75. Jeffrey A Hutchings. Influence of growth and survival costs of reproduction on atlantic cod, *Gadus morhua*, population growth rate. *Canadian Journal of Fisheries and Aquatic Sciences*, 56(9):1612–1623, 1999. ISSN 0706-652X.
76. Robert NM Ahrens, Carl J Walters, and Villy Christensen. Foraging arena theory. *Fish and fisheries*, 13(1):41–59, 2012. ISSN 1467-2979.
77. Yang Xiang, Sylvain Gubian, Brian Suomela, and Julia Hoeng. Generalized simulated annealing for global optimization: The GenSA package. *R J.*, 5(1):13–28, 2013. ISSN 20734859. doi: 10.32614/rj-2013-002.
78. Rainer Storn and Kenneth Price. Differential Evolution - A Simple and Efficient Heuristic for Global Optimization over Continuous Spaces. *J. Glob. Optim.*, 11:341–359, 1997. doi: 10.1023/A:1008202821328.

DRAFT

SI Appendix
Supplementary Information
"Size-selective mortality may trigger maladaptive changes of shoaling behaviour in a fish"

Valerio Sbragaglia[a,b,1,2], Pascal P. Klamser[c,d,1], Pawel Romanczuk[c,d,3], Robert Arlinghaus[a,e]

a Department of Biology and Ecology of Fishes, Leibniz-Institute of Freshwater Ecology and Inland Fisheries, Müggelseedamm 310, 12587 Berlin, Germany
b Department of Marine Renewable Resources, Marine Science Institute (ICM-CSIC), Barcelona, Spain
c Department of Biology, Institute for Theoretical Biology, Humboldt-Universität zu Berlin, 10115 Berlin, Germany
d Bernstein Center for Computational Neuroscience, 10115 Berlin, Germany
e Division of Integrative Fisheries Management, Department of Crop and Animal Sciences, Faculty of Life Science, Humboldt-Universität zu Berlin, Invalidenstrasse 42, 10115 Berlin, Germany

[1] V.S. and P.P.K. contributed equally to this work.
Correspondence:
[2]experimental data: valeriosbra@gmail.com
[3]models and simulations: pawel.romanczuk@hu-berlin.de

DRAFT

I Model description

The burst-coast model intends to mimic the burst-coast swimming behavior of zebrafish (*Danio Rerio*). We assume that a fish is accelerating only during the burst phase with a constant force of magnitude f_b, while no forces are present during the coast phase implying a deceleration due to friction. The differential equations of motion defining current position $\vec{r}_i$ and velocity $\vec{v}_i$ of an agent i are:

$$\frac{d\vec{r}_i}{dt} = \vec{v}_i \tag{S1a}$$

$$\frac{d\vec{v}_i}{dt} = -\beta\vec{v}_i + \vec{F}_i(t) \tag{S1b}$$

with $\vec{F}_i(t)$ as a finite social or environmental force vector with $|F(t)| > 0$, for fish in the bursting phase. A fish decelerates passively during the coasting phase, thus the force vector vanishes $|\vec{F}_i| = 0$. β is the friction coefficient. The velocity change of Eq.(S1) can be split into the part parallel and perpendicular to the current velocity direction $\vec{v} = v[cos(\varphi), sin(\varphi)]$:

$$\frac{d\vec{v}}{dt} = \frac{dv}{dt}\vec{e}_r + v\vec{e}_\varphi\frac{d\varphi}{dt} \tag{S2a}$$

$$\frac{dv_i}{dt} = -\beta v_i + \vec{F}_i \cdot \hat{e}_r \tag{S2b}$$

$$\frac{d\varphi_i}{dt} = \frac{1}{v}\vec{F}_i \cdot \hat{e}_\varphi \ . \tag{S2c}$$

Note that the v^{-1} dependence of the turning rate (Eq. S2c) follows directly from Eq. S1b via a coordinate transformation (51). In addition it has been verified by experimental tracking data (Fig. S4).
The burst behavior is defined by the burst rate γ, the burst time or duration of the burst t_b, and the burst force $\vec{F}$. In particular the burst force $\vec{F}$ governs whether the fish uses social or environmental cues. The fish decides at the start of a burst with a probability P_{social} if reacting socially to the other fish or, with probability $1 - P_{social}$, to environmental cues.
The resulting burst force $\vec{F}$ is

$$\vec{F} = \begin{cases} F\hat{f}_{soc}, & \text{if } p < P_{soc} \text{ with } p \sim U(0,1) \\ F\hat{f}_{env}, & \text{otherwise} \end{cases} \tag{S3}$$

with F as the magnitude of the burst force and $\hat{f}_{env}$, $\hat{f}_{soc}$ as the unit vectors in direction of the environmental or social cue.

I. A. Social forces. The social force is motivated by a three zone model (22) consisting of a repulsion zone vanishing at a distance r_r, followed by the alignment zone vanishing at r_o, and the attraction zone vanishing at r_a. Thus, $r_r < r_o < r_a$. The direction of the social forces is computed by

$$\hat{f}_{i,rep} = \mathcal{N}\left(\sum_{j\in\mathbb{S}_{i,r}} -\hat{r}_{ji}\right) \tag{S4a}$$

$$\hat{f}_{i,alg} = \mathcal{N}\left(\sum_{j\in\mathbb{S}_{i,o}} \vec{v}_{ji}\right) \tag{S4b}$$

$$\hat{f}_{i,att} = \mathcal{N}\left(\sum_{j\in\mathbb{S}_{i,a}} \hat{r}_{ji}\right) \tag{S4c}$$

with $\hat{x} = \vec{x}/|x|$ defining a unit vector, $\vec{x}_{ji} = \vec{x}_j - \vec{x}_i$ as the difference between the vectors of fish j and i, $\mathbb{S}_{i,x}$ is the set of indices of fish in zone x of fish i, and $\mathcal{N}(\vec{x}) = \hat{x}$ is a normalization operator. We assume Voronoi interactions because they provide a reasonable approximation to visual networks (52) and can be efficiently computed. Therefore, the sets $\mathbb{S}_{i,x}$ with $x \in [r, o, a]$ are composed only of Voronoi neighbors of fish i. Note that the alignment force is the sum of the velocity difference vectors $\vec{v}_{ji}$. Thus, the focal fish i experiences the strongest alignment with neighbours whose velocity vectors differed the most from its own.

If neighbors of fish i occupy different zones simultaneously the following rules apply:

- if $\mathbb{S}_r \neq \emptyset$: $\hat{f}_{soc} = \hat{f}_r$ (repulsion dominated)
- if $\mathbb{S}_r = \emptyset$ and $\mathbb{S}_o \neq \emptyset$ and $\mathbb{S}_a \neq \emptyset$: $\hat{f}_{soc} = \mathcal{N}(|\mathbb{S}_a|\hat{f}_a + |\mathbb{S}_o|\hat{f}_o)$ (weighted average)

I. B. Environmental force. In the absence of a predator the environmental force is modelled as a random force vector. This models the sensitivity of individual fish to environmental noise (e.g. water reflections, water perturbations, sounds), and to a resulting false-positive escape response. In the presence of a threatening agent the environmental force is modelled as a simple repulsion of the shoaling fish from the simulated predator or fishing agents

$$\hat{f}_{env} = \begin{cases} [cos(\varphi), sin(\varphi)] \text{ with } \varphi \sim U(-\Pi, \Pi) & \text{no predator present, } \mathbb{S}_{i,p} = \emptyset \\ \mathcal{N}\left(\sum_{p\in\mathbb{S}_{i,p}} -\hat{r}_{pi}\right) & \text{otherwise} \end{cases} \tag{S5}$$

with $U(a, b)$ being a uniform distribution with a and b as lower and upper bounds, and $\mathbb{S}_{i,p}$ being the set of predator or fishing agents detected by a shoaling fish i. A predator or fishing agent is detected by a shoaling fish with probability

$$P_{detect} = \frac{2}{1 + r_{pi}/r_f} \tag{S6}$$

which equals one at $r_{pi} = r_f$. If $P_{detect} > 1$ it is set to 1. r_f is the detection distance which was for all simulations $r_f = 7\ cm$. This value is reasonable because fish should be able to detect a predator when they are likely to be captured $r_f \geq r_{capture} = 5\ cm$ but the distance should also be close to $r_{capture}$, otherwise fish would respond too often to non-dangerous cues and because the visibility in water decays with distance. The randomness is a consequence of the assumption that shoaling fish misinterpret reflections on the water surface as threats since there were no "real" threats in the experiment.

I. C. Wall-avoidance mechanism. We attempt to design the model as close to the experimental setting as possible and therefore use a circle as a boundary. The introduction of parameters describing the repulsion force from the wall was avoided by the fish following a parameter free wall-avoidance mechanism. It is based on predicting before each burst the future position $\vec{r}(t_1)$ of the shoaling fish at the next burst (at t_tnb which stands for "time to next burst") plus some extra time (at time $t_1 = t_{tnb} + t_b$). The extra time t_b is necessary because the agent can not prevent collision with the finite burst force, if it is at the next burst inside the tank but directly at, or very close to the wall. The length of the extra time is set to the burst time t_b, because if the agent coasts (i.e. uses no force) and does not collide with the wall, any burst force is sufficient to prevent collision if the agents bursts instead. If the predicted position $\vec{r}(t_1)$ is outside of the tank, the force direction is adapted until $\vec{r}(t_1)$ is inside the tank. Thereby is the smallest possible change in force direction used. This ensures that the shoaling fish avoids the wall while pursuing its intended direction.

To predict the future position $\vec{r}(t_1)$ with $t_1 = t_tnb + t_b$ the solution of the coupled differential Eq. S1 for $\vec{v}(t)$ and $\vec{r}(t)$ are used. Since the x and y components of $\vec{v}(t)$ and $\vec{r}(t)$ are not coupled with each other, the solutions are computed for each component

DRAFT

seperately:

$$v(t) = (v_0 - F/\beta)e^{-\beta t} + F/\beta \tag{S7a}$$

$$r(t) = \frac{1}{\beta}(v_0 - \frac{F}{\beta})(1 - e^{-\beta t}) + \frac{F\,t}{\beta} \tag{S7b}$$

where I omitted the index r_x or r_y for the terms r, F, v_0 and v for simplicity. The solutions above assume a constant force F. Therefore, first, the position and velocity after the burst are predicted and then, second, the position after the coast.

I. D. Capture probability of a single fish by a natural predator. If a shoaling fish is closer to the predator than $r_{capture}$ its probability to be successfully captured within a small time window $[t, t+\delta t]$ is

$$p_{success}(t, \delta t) = p_{confuse}(t) \cdot \gamma_a \delta t. \tag{S8}$$

Here γ_a is the predator attack rate, and $p_{confuse}(t)$ represents the confusion effect that modulates the attack rate. The attack rate used in the simulations is $\gamma_a = 1/s$. The confusion term depends on the spatial configuration of shoaling fish around the predator and decreases $p_{success}$ the more individuals are sensed (55). A shoaling fish is sensed if it is closer than $r_{sense} = 4 \cdot r_{capture}$. We assume that it modulates the successful capture probability in a sigmoidal way depending on the number of sensed shoaling fish N_{sensed}:

$$p_{confuse} = \frac{\tanh(-(N_{sensed} - N_{conf})) + 1}{2}. \tag{S9}$$

Here $N_{conf} = 4$ is the number of sensed shoaling fish at which $p_{confuse} = 0.5$.

I. E. Random movement of angling agent with constant persistence length. The individual fishing agent is supposed to have a constant persistence length. It's angular change is given by

$$\frac{d\varphi}{dt} = \hat{\sigma}_\varphi \xi(t). \tag{S10}$$

$\xi(t) \propto \mathbb{N}(0,1)$ is Gaussian white noise with zero mean and variance of one. $\hat{\sigma} = \hat{\sigma}(v_{net})$ is the angular noise strength whose exact form and dependence is derived below.
Keeping the persistence length constant is equivalent with keeping the variance in angle constant after the individual fishing agent travelled a path of length = l. The time needed to travel this path-length is $t_l = l/v_f$ and the variance in angle after travelling the path is

$$Var(\varphi)(l, v_{net}) = \langle \varphi(l, v_{net})^2 \rangle \tag{S11a}$$

$$= \langle \left(\int_0^{t_l} \hat{\sigma}_\varphi \xi(t) dt \right)^2 \rangle = \hat{\sigma}_\varphi^2 \int_0^{t_l} \int_0^{t_l} \langle \xi(t)\xi(t') \rangle dt dt' \tag{S11b}$$

$$= \hat{\sigma}_\varphi^2 \int_0^{t_l} \int_0^{t_l} \delta_{t,t'} dt dt' = \hat{\sigma}_\varphi^2 \int_0^{t_l} dt \tag{S11c}$$

$$= \hat{\sigma}_\varphi^2 t_l = \hat{\sigma}_\varphi^2 \frac{l}{v_{net}}. \tag{S11d}$$

Here we used that the Gaussian white noise is uncorrelated, e.g. $\langle \xi(t)\xi(t') \rangle = \delta_{t,t'}$, with $\delta_{t,t'}$ as the Kronecker-delta. If we set $\hat{\sigma}_\varphi = \sigma_\varphi \cdot \sqrt{v_{net}}$, the variance in angle after travelling a path of length l is independent of the speed:

$$Var(\varphi)(l) = \hat{\sigma}_\varphi^2 \frac{l}{v_{net}} \tag{S12a}$$

$$= \sigma_\varphi^2 \cdot l. \tag{S12b}$$

II Parameter setting

The model has in total eight parameter, from which six can be estimated from experimental measures without the need to simulate the model. The remaining two parameter can not directly be accessed from data and were estimated by an optimization. The optimization minimized the sum of squared differences between model emergent properties and their experimental measured values. For an overview of all model-parameters and how they are set see Fig. S2A. First, section II. A explains the simulation-free parameter estimation from experimental measures in detail. Second, section II. B explains the optimization of the remaining parameters by comparing model emergent measures. All model parameters are summarized in Tab. S1.

DRAFT

II. A. Simulation-free parameter estimation. Since in the model (see section I) an agent can be either in the burst or coast phase we split individual trajectories in these phases. Burst and coast phases are characterized by an increase and decrease in the speed of the shoaling fish, respectively. In the coast phase the only parameter which defines change in velocity is the **friction coefficient** β (Eq. S2). Thus, we estimated $\beta = 2.51$ by the slope of the linear regression between the response in speed to the current speed of the fish during coast-phases as seen in Fig. S5. Because the friction force is by definition zero at zero velocity we fixed the interception point to zero and therefore found effectively the least-square solution of the linear equation $\frac{dv}{dt} = -bv$. We assumed the same friction coefficient β for the model representations of all selection lines because, first, β is based on Stokes law for which the β depends on the cross-section of the fish perpendicular to its moving direction. The size differences between selection lines could in principle change the friction (larger individuals have a larger cross section and therefore a larger friction coefficient), but the differences probably negligible. Note, that we also assume the same mass for all selection lines and therefore could different average masses also influence the effective friction (which is strictly the friction divided by the assumed mass). Second, even if they are not negligible or differ in mass, a lower friction coefficient does impact the speed in the model as does the burst-force. Thus, by allowing the burst force to vary between selection lines we effectively take account for differences in the friction coefficient.

The average **burst duration** $\langle t_b \rangle$ and **rate** $\langle \gamma \rangle$ were estimated by the mean length and frequency of burst periods. For the large-, random- and small-harvested line the burst duration was $\langle t_b \rangle = [0.117, 0.123, 0.123]s$ and the burst rate was $\langle \gamma \rangle = [0.35, 0.44, 0.38]$ respectively. In the model a new burst period can start during an already ongoing burst and therefore prolong the measured burst duration and decrease the rate, as illustrated in Fig. S2D. Consequently is the average burst duration and rate different from the model-parameters t_b and γ. We approximated them by creating a binary time series in which at each time-step dt a burst-event happens with probability $\gamma * dt$ which raises the acceleration from zero to F for a duration of t_b. We simulated this process, computed the average values $\rangle t_b \langle_N$, $\rangle \gamma \langle_N$ (as seen in Fig. S2D) and selected the γ and t_b which minimized the summed square differences to the experimental observed averages for each harvested line. In Fig. S1 the squared differences are shown. The resulting parameters are reported in Tab. S1.

The **burst force** F in heading direction $f_{b,s}$ can be estimated by adding to the change in speed $\frac{dv}{dt}$ the friction coefficient times the current velocity $\beta \cdot v$. This results in the mean burst force in heading direction $f_{b,s} = 95cm/s^2$. However, from Eq. S2 it is clear that the total magnitude of the burst force is defined as

$$f_b = \sqrt{f_{b,s}^2 + f_{b,\varphi}^2} \tag{S13}$$

with $f_{b,\varphi} = \frac{d\varphi}{dt} \cdot v$ (from Eq. S2c). Note, that we are using f_b instead of the symbol for the model parameter F because we expect F to be larger than f_b since the latter is estimated from forces only during the burst-phase. However, the turning force often started prior to the acceleration in velocity direction and reached its maximum at the start of the burst (Fig. S6C, D). This suggests that the actual force F needed to mimic the characteristic zigzag-like swimming of zebrafish is larger than f_b. For the different selection lines we estimated $\langle f_{b,LH} \rangle = 121.2cm/s^2$, $\langle f_{b,RH} \rangle = 135.2cm/s^2$, $\langle f_{b,SH} \rangle = 102.3cm/s^2$. Thus, instead of setting $F = f_b$ we used its largest mean to set the boundaries of the search-space for F in the optimizer.

The **ranges of the social-interactions zones** (r_r, r_o, r_a) are set to minimize the angle between the predicted and the actual direction after a burst (see Fig.S2C). The computation of the predicted direction is based on the relative positions of neighbors of the focal, bursting fish at the start of the burst. From this neighbor constellation the direction of the social force is computed with Eq.S4a. This is done for each burst-event in which the bursting fish was at least three body length away from the tank wall. How well a given choice of interaction zone ranges explains the data was estimated by the mean angle difference between its predicted and the actual direction after the burst. To find the parameter-choice for r_r, r_o and r_a which minimizes this angle difference we, first, ran two different optimizer (dual-annealing: python/scipy implementation of (77), differential-evolution: python/scipy implementation of (78)) which gave for each selection line similar parameters. For all selection lines the width of the orientation zone was below 2 millimeters which suggests that the best solution favors no alignment at all. To verify this we did two-dimensional parameter scans around the optimal parameter setting (see Fig.S10). For the scan in which the repulsion r_r and orientation range r_o are varied, the angular difference is lowest if $r_o = r_r$, i.e. for a two-zone model without orientation zone(Fig.S10B, E, H). Consequently we set the $r_o = r_r$ and did a parameter-scan (Fig.S11) around the optima of the selection lines. From this scan we extracted the ranges reported in Tab.S1. Interestingly are the ranges of the large-harvested line smaller than the ones of the random-harvested line which again are smaller than the ones of the small-harvested line. Therefore, the ranges can be interpreted to represent body-length differences in between the selection lines.

II. B. Parameter setting by fitting emergent variables. To fit the model to the data we applied the CMA-ES (53, 54). This optimizer is a good choice if the fitness landscape is multi-modal, the search space dimension is between 4 and 100 and no gradient is known. The optimizer minimizes the error function

$$E(\mathbb{P}_{LH}, \mathbb{P}_{RH}, \mathbb{P}_{SH}) = \frac{Err(\mathbb{P}_{LH}) + Err(\mathbb{P}_{RH}) + Err(\mathbb{P}_{SH})}{3} \tag{S14}$$

DRAFT

with $\mathbb{P}_{\text{SL}}$ as the set of parameter of a selection line (SL) needed to run a simulation. Eq. S14 averages over the selection line errors. The error of a specific selection lines compares the measured nearest neighbour distance NND and average individual speed v to the experimental data by computing the sum of the squared differences standardized by their experimental standard deviation:

$$Err(\mathbb{P}_{\text{SL}}) = \left(\frac{\langle \text{NND} \rangle_{\text{SL}} - \langle \text{NND} \rangle_{M,\text{SL}}}{\sigma_{\text{NND, SL}}} \right)^2 + \left(\frac{(\langle v \rangle_{\text{SL}} - \langle v \rangle_{M,\text{SL}}}{\sigma_{v,\text{SL}}} \right)^2 . \tag{S15}$$

Here the index M in $\langle \text{x} \rangle_{M,\text{SL}}$ marks that the measure of x is based on model simulations. $\langle \text{x} \rangle_{\text{SL}}$ and $\sigma_{x,\text{SL}}$ are the experimental mean and standard deviation of the measure x. SL specifies the selection line. The experimental means of NND and v used for the error function are listed in Tab. S2.

At each generation the parameter sets are updated by the CMA-ES. Note that the parameter sets differ in burst-duration, -rate, repulsion-, attraction-range and probability to respond to social cues in between the selection lines. In the sections before we already defined most parameter from data. Only the burst force F and the probability to respond to social cues needs setting. Consequently the search-space is 6-dimensional ($P_{soc,LH}$, $P_{soc,RH}$, $P_{soc,SH}$, F_{LH}, F_{RH}, F_{SH}) as highlighted in Tab. S1.

We limited the search-space of the algorithm for the three different parameters by setting boundaries which are listed in Tab. S2. For the probability to follow social cues we ensured a minimum attention to social and environmental cues by setting the boundaries 0.05 above and below the theoretical possible boundaries of zero and 1. We expect the burst force to be larger than the experimentally estimated measure. Therefore, its boundaries are half and twice the mean burst force of the random harvested line, as in section II. A.

To ensure that the resulting minimum is not a local minimum we repeated the optimization from different initial parameter settings. The initial parameter were selected from a two-dimensional grid with 2 grid-points and therefore $2^2 = 4$ different initial parameter settings. Note that the actual search-space is 6-dimensional and by setting P_{soc} and F for the different selection line initially equal we reduce the number of initial settings from $2^6 = 64$ to 4.

An example optimization run over 400 generations is shown in Fig. S8. The optimization outcomes of the 4 different initialization are shown sorted by their final error according to Eq. S14 in Fig. S9.

III Mean distance of shoaling fish to fishing agents

Here we computed the mean distance the shoaling fish kept from fishing agents. This measure is an alternative to the exploitation rate used in the main text, to quantify how well the shoaling fish avoid capture:

$$\langle d_{if} \rangle = \frac{1}{N} \sum_{i=1}^{N} \min_{f \in \mathbb{S}_f} d_{if} \tag{S16}$$

with $d_{if} = |\vec{r}_{if}|$ as the distance between shoaling fish i and a fishing agent f. The minimum function yields the distance to the closest fishing agent. In Fig. S3I, J, K, L show the relative and M, N, O, P the normal mean distance to the predator. The distance measured substantiated the already reported results for the exploitation rate. Note that in the natural-predator scenario (I, M) the differences between selection lines is qualitatively equivalent to the other scenarios in contrast to the scenario comparison with the exploitation rate(A, E). This is due to (i) the confusion effect, the main difference between the natural predator and the other fishing agents, which reduces the exploitation rate for more cohesive shoals (RH and SH line) but does not affect the distance and (ii) the fast individual speed of the RH line, which enables the currently pursued fish to better escape but has no effect on how the other shoaling agents detect and avoid the predator. Note that the natural predator moves at constant speed and is therefore only on average faster than the shoaling fish.

IV Movies

Movie-S1.avi. Eight shoaling fish are simulated in a circular area with fitted social interaction. The parameters were the ones estimated for the random harvested line listed in Tab. S1.

Movie-S2.avi. This movie shows simulations in the circular area with parameters adjusted such that only the wall avoidance mechanism changes the path of the shoaling fish. The parameters are the ones estimated for the random harvested line listed in Tab. S1 apart for the repulsion, alignment and attraction range and probability to follow social cues P_{soc}. Those parameters were set such that the agents always responded to social information $P_{soc} = 1$, but never had any neighbors due to short ranges $r_r = r_o = r_a = 0.001cm$. Thus, the agents effectively swim always straight until they come in conflict with the wall. Then the wall avoidance mechanism started.

DRAFT

Movie-S3.avi. Thirty agents simulated in a rectangle of length $L = 100cm$ with periodic boundary conditions in the predator scenario. The parameters were the ones estimated for the random harvested line listed in Tab. S1 and additional fishing/predator scenario parameters listed in Tab. S3. Note that the predator, in red, moves with a speed of $v_p = 20cm/s$ and therefore faster as the average velocity of shoaling fish. However, it moves directly to the closest prey and therefore covers the prey until it get killed. Due to the confusion effect the killing probability was lowered and it happens that the predator stays for a notable time above the targeted fish.

Movie-S4.avi. Thirty agents simulated in a rectangle of length $L = 100cm$ with periodic boundary conditions in the angler scenario. The parameters were the ones estimated for the random harvested line listed in Tab. S1 and additional fishing/predator scenario parameters listed in Tab. S3.

Movie-S5.avi. Thirty agents simulated in a rectangle of length $L = 100cm$ with periodic boundary conditions in the trawling scenario. The parameters were the ones estimated for the random harvested line listed in Tab. S1 and additional fishing/predator scenario parameters listed in Tab. S3.

DRAFT

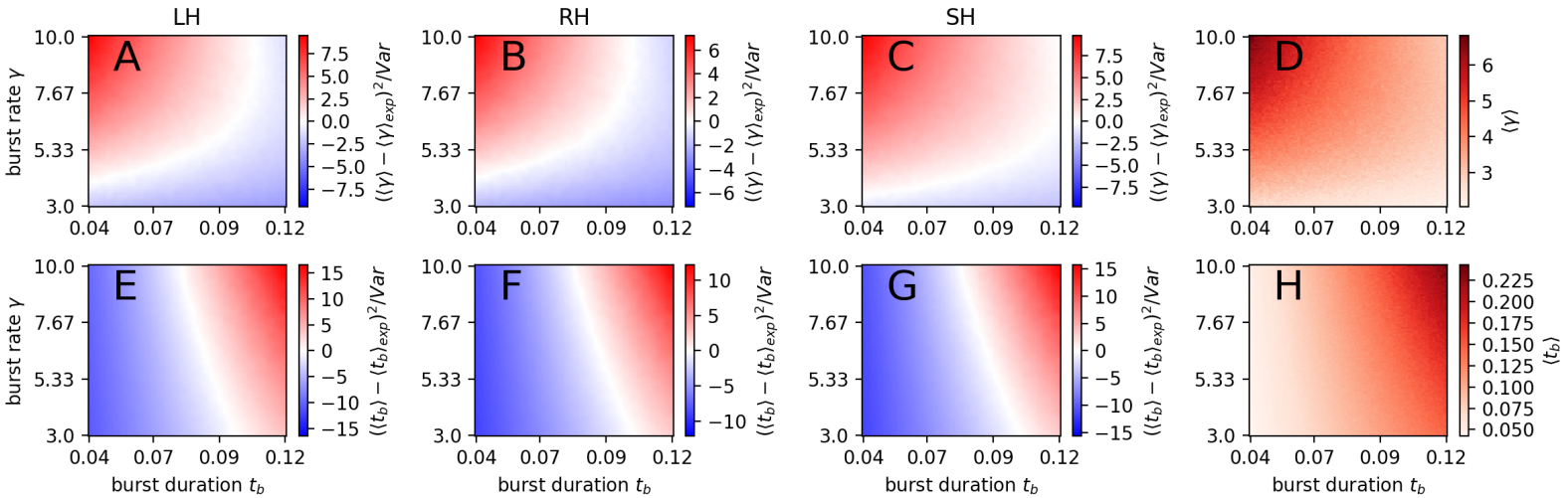

Fig. S1. Model parameter estimation of burst duration t_b and burst rate γ (parameters of an acceleration-time-series generating model). The acceleration-based-average is reported for burst rate $\langle\gamma\rangle$ (**A-D**) and burst duration (**E-H**) $\langle t_b\rangle$. The normalized squared difference between the averaged values of the simulation $\langle x\rangle$ and the experiment $\langle x\rangle_{exp}$ are shown for large-harvested line (LH; **A, E**), random-harvested line (RH; **B, F**) and small-harvested line (SH;**C, G**). The normalization was done by dividing the squared differences by the experimental variance of the burst rate (**A-C**) or of the burst duration (**E-G**). The average values of the simulation are shown in (**D, H**).

DRAFT

model parameter	symbol	estimated value	estimation method	unit
repulsion range	r_r	LH: 3.92 RH: 4.44 SH: 4.71	data+model	cm
alignment range	r_o	r_r	data+model	cm
attraction range	r_a	LH: 15.84 RH: 18.45 LH: 19.5	data+model	cm
burst force	F	LH: 215.1 RH: 234.4 SH: 193	optimizer	cm/s^2
prob. of social burst	P_{soc}	LH: 0.5 RH: 0.71 SH: 0.74	optimizer	1
burst duration	t_b	LH: 0.089 RH: 0.091 SH: 0.097	data+model	s
burst rate	γ	LH: 5.7 RH: 6.3 SH: 4.7	data+model	$1/s$
friction coefficient	β	2.51	data	$1/s$

Table S1. Model parameters of the burst-coast model and their estimates. The estimation methods are colored according to the colors used in Fig. S2A. Each selection line has its specific parameter, but the friction coefficient β which is the same for all lines, which is indicated by the abbreviations LH: large-harvested; RH: random-harvested and SH: small-harvested.

optimization parameter	symbol	optimization boundaries	unit
burst force	F	$[67.6,\ 270.4]$ $(=[\langle f_b\rangle_{RH}/2,\ 2\langle f_b\rangle_{RH}\ )$	cm/s^2
prob. of social burst	P_{soc}	$[0.05,\ 0.95]$	1
error function defining measures	**symbol**	**experimental mean and STD**	**unit**
individual speed	v	LH: 15 ± 2.8 RH: 17 ± 2.5 SH: 13.2 ± 2.7	cm/s
nearest neighbor dist.	NND	LH: 6.4 ± 1 RH: 5.8 ± 1.1 SH: 5.6 ± 0.9	cm

Table S2. The upper part of the table lists the upper and lower boundaries in which the optimizer searched for the minimum of the error function Eq. S14. The lower and upper boundary of the burst force F are given by half and twice the mean of the experimental estimated burst force $\langle f_b\rangle_{RH}$ of the RH line. The lower part of the table lists the measures defining the error function Eq. S14 which is minimized by the optimizer.

scenario related parameter	symbol	value	scenario relevance	unit
flee range[a]	r_f	7	all	cm
fishers/predators capture range	$r_{capture}$	5	all	cm
predators sensing range	r_{sense}	$4r_{capture} = 20$	natural pred.	cm
confusion number	N_{conf}	4	natural pred.	cm
attack rate	γ_a	1	natural pred.	$1/s$
angular noise strength	σ_φ	0.2	single fisher	$1/s^{1/2}$

Table S3. Parameters used to simulate interaction of fish with predator/fisher in different scenarios. The column "scenario relevance" specifies for which scenario the parameter is needed. [a]: Note that the flee range influences the probability of a prey detecting a predator/fisher (Eq. S6) which is 0.5 at a distance of $21cm$ given $r_f = 7cm$. Therefore, the range of the prey to detect a predator is comparable to the predators sensing range.

DRAFT

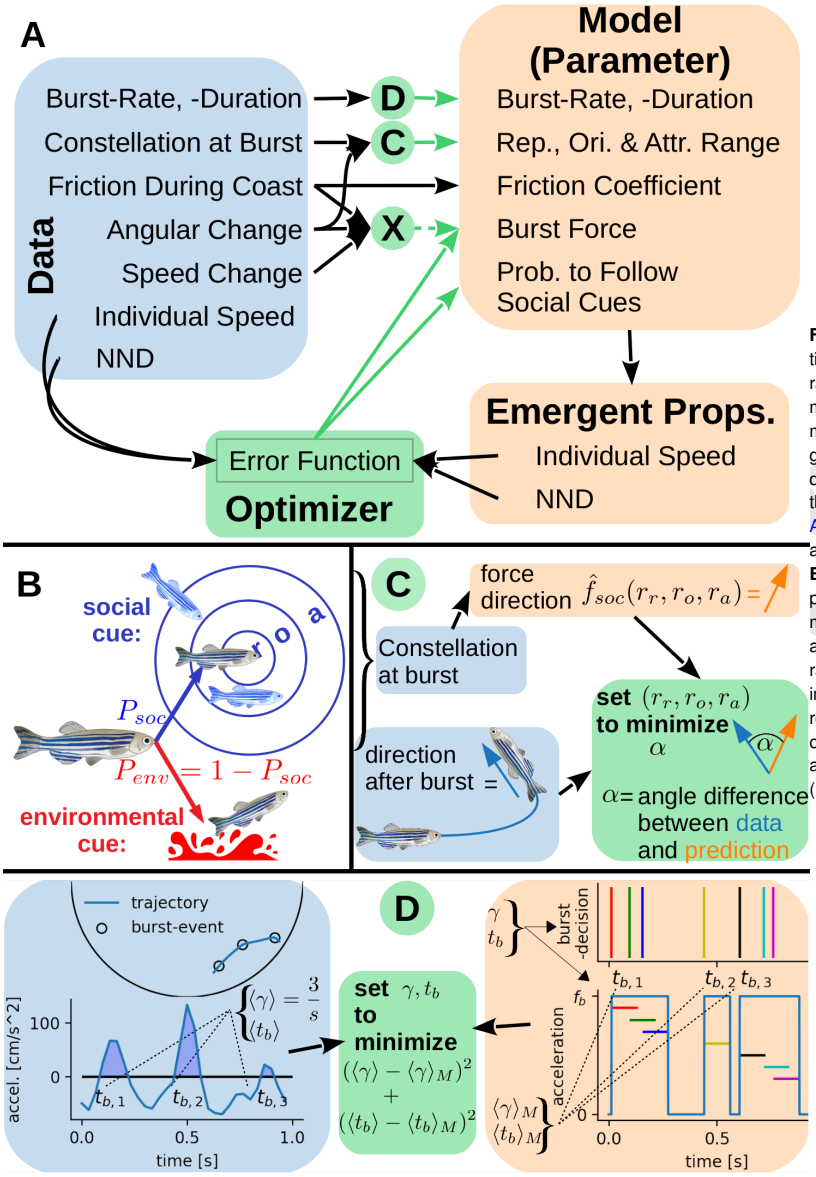

Fig. S2. Summary of model parameter setting from data. **A**: relations between trajectory data based measurements and model parameters. All light green boxes/circles represent optimizer which minimize an error-function by adjusting the model parameters. The model parameter setting is indicated by green arrows. The central green circle marked with an "X" represents the optimizer which deduces the burst force parameter. However, since our estimation of the burst force F is likely to be too low (as explained in Sect. II. A) and therefore is estimated by the optimizer which compares NND and speed, we omit an illustrative explanation of its dependence. **B**: model scheme of burst decisions. An individual can follow with probability P_{soc} social cues (i.e. behaves according to a three-zone model: r=repulsion-, o=orientation-, a=attraction-zone) or with probability $P_{env} = 1 - P_{soc}$ environmental cues. **C**: sketch of how the range of repulsion r_r, orientation r_o, and attraction r_a are set by minimizing the angle difference α between the model-predicted force direction $\hat{f}_{soc}$ and the actual heading direction after a burst. **D**: setting of the burst rate γ and duration t_b. The difference between the averages based on data ($\langle\gamma\rangle$, $\langle t_b\rangle$ blue box) and on model-simulations ($\langle\gamma\rangle_M$, $\langle t_b\rangle_M$ orange box) is minimized.

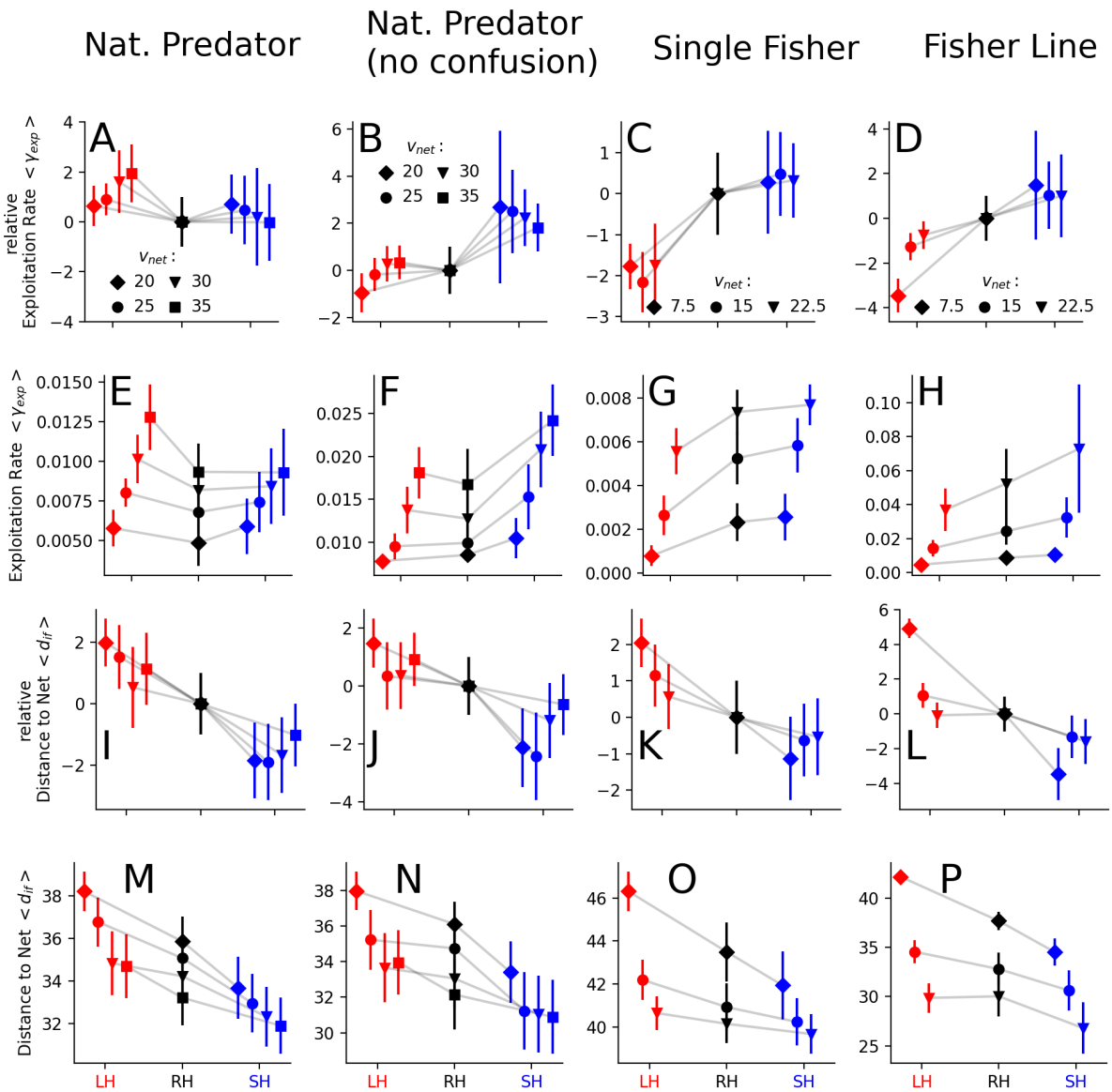

Fig. S3. The relative (**A-D**) and normal (**E-H**) mean exploitation rate γ_{exp} and the relative (**I-L**) and normal (**M-P**) mean distance to the closest fishing agent d_{if} are shown for different scenarios. The relative measures were computed by reducing the selection line means by the mean and dividing them by the standard deviation of the random-harvested line. In the "natural predator" scenario a predator pursues the closest shoaling fish with different speeds $v_{net} = [20,\ 25,\ 30,\ 35]\ cm/s$ but its capture success is reduced the more prey it senses, i.e. by the confusion effect (1st column, **A, E, I, M**). The "natural predator without confusion" scenario is the same but without the confusion effect (2nd column, **B, F, J, N**). In the "single fisher" scenario an uninformed single fisher moves randomly and captures shoaling agents at encounter (3rd column, **C, G, K, O**). In the "multiple fishing agent" scenario fishing agents move $N_f = 50$ fishing agent on a rigid line towards the center of mass of the fish shoal (4th column, **D, H, L, P**). The speed of the fishing agents in the "single fisher" and "mutliple fishing agent" scenarios was $v_{net} = [7.5,\ 15,\ 22.5]\ cm/s$ indicated by rhombus, circle, triangle, respectively. In all simulations $N = 30$ shoaling fish moved in a box of size $L = 100\ cm$ with periodic boundary conditions. Their mean individual speed was about $\langle v \rangle \approx 15\ cm/s$. The symbols and error bars represent the mean and standard deviation computed from samples of 400 simulations.

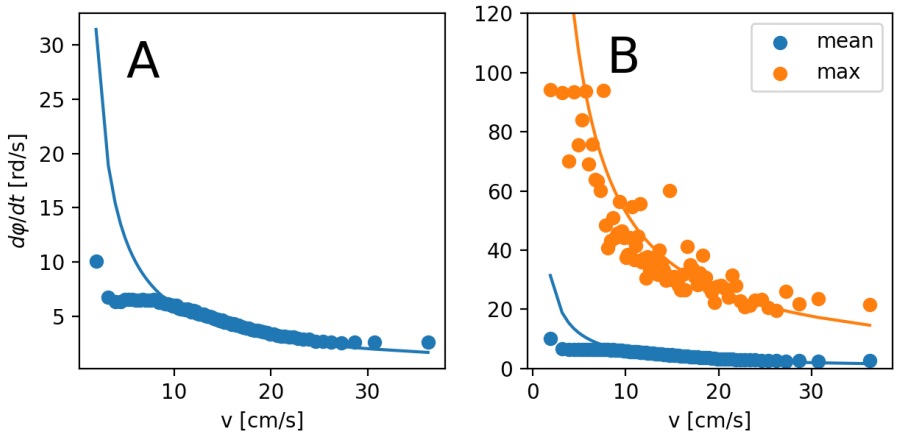

Fig. S4. Angular change $d\varphi/dt$ depending on the velocity v. The blue dots (**A, B**) represent the mean values while orange dots (**B**) the maximum observed value for the binned data. The lines are not fitted to the data but serve as an comparison to the inverse proportionality. The blue line is $f(v) = 6/v$ and the orange line is $f(v) = 530/v$. The resemblance of the data to the lines supports the model assumption in Eq. (S2c).

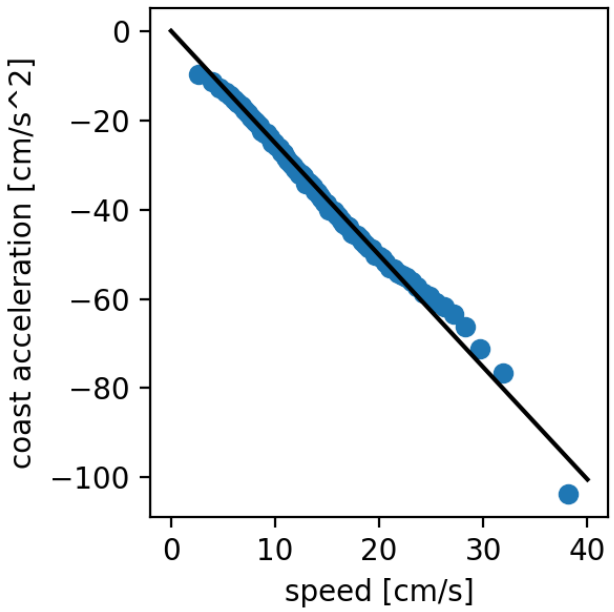

Fig. S5. Estimation of friction coefficient from experimental data. Dots represent mean of bins with varying width such that each bin contains an equal amount of data. Black line shows linear fit with the interception at zero and the negative friction coefficient as slope $-\beta = -2.51$.

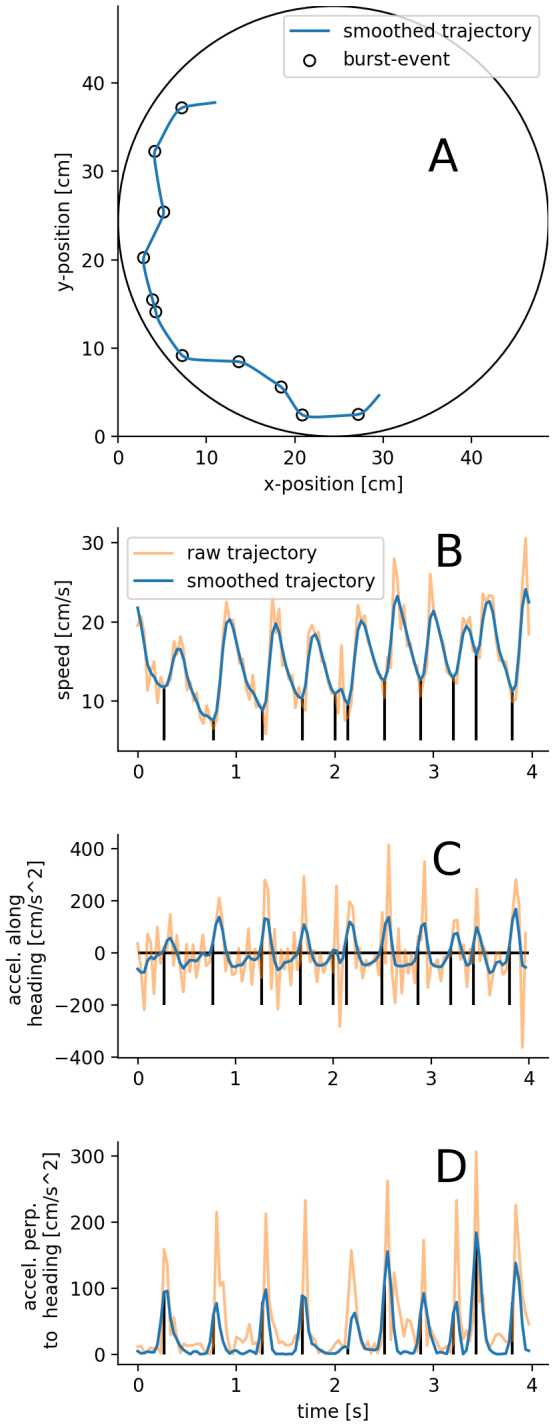

Fig. S6. Example smoothed trajectory of a swimming zebrafish generated from ID-Tracker data (**A**). The large circle represents tank-boundary. For this trajectory the speed (**B**), acceleration along (**C**) and perpendicular (**D**) to heading direction are shown computed from the raw (orange) and smoothed (blue) trajectory. The black circles (**A**) and vertical black lines (**B, C, D**) indicate burst events which are are the onsets of a positive acceleration period of the smoothed data (**C**). For the smoothening a moving window average with gaussian kernel was used. The kernel width $\sigma_{smoo} = 1.13fms$ was estimated by comparing manual counts of burst events with automatically detected (see Fig. S7).

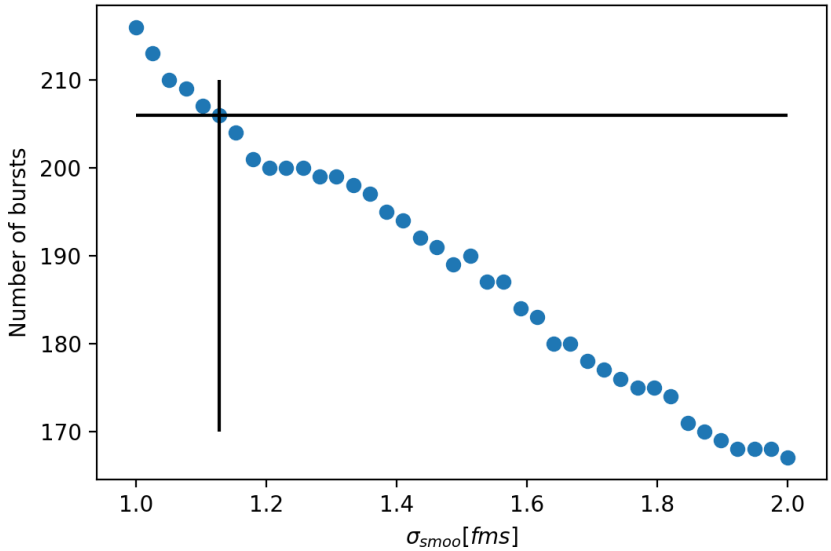

Fig. S7. Number of burst events of a randomly selected trajectory spanning 2000 frames. The horizontal black line marks the number of manually counted burst events. Blue dots mark automatic counts of burst events on a smoothed trajectory using a moving window with a Gaussian kernel of varying standard deviation σ_{smoo}. The vertical black line indicates the standard deviation $\sigma_{smoo} = 1.13\ fms$ where the number of automatically detected bursts equals the manually counted one in an interval of 2000 frames.

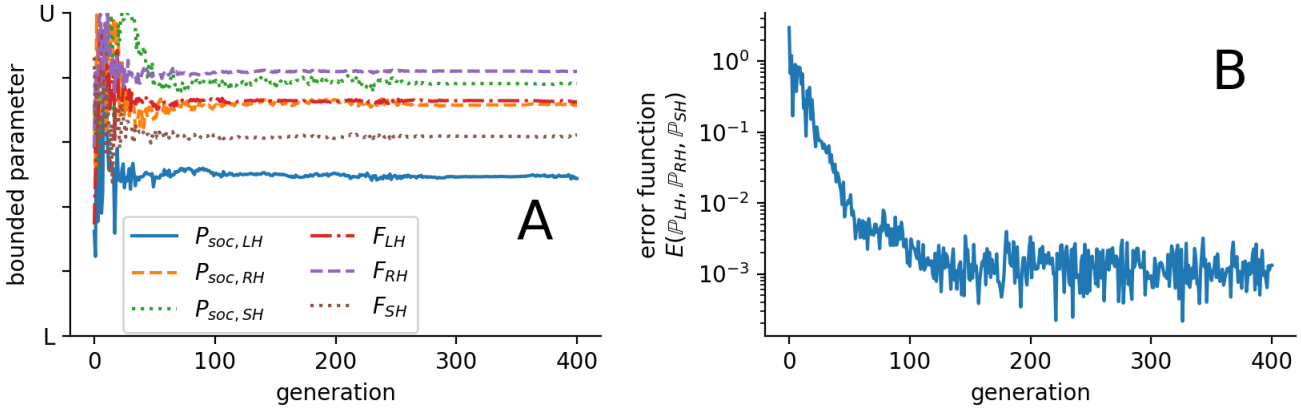

Fig. S8. Example of optimization run with the parameters which result in the lowest error in the current generation (**A**) and the corresponding error (**B**). The parameters are normalized according to their respective lower and upper boundary (see Tab. S2) which are marked on the y-axis with L and U (**A**). Different colors and linestyles mark the probability to respond to social cues P_{soc} of the large (solid blue), random (dashed orange) and small (dotted green) harvested line and the burst forces F of the large (dash dotted red), random (dashed violet) and small (dotted brown) harvested line.

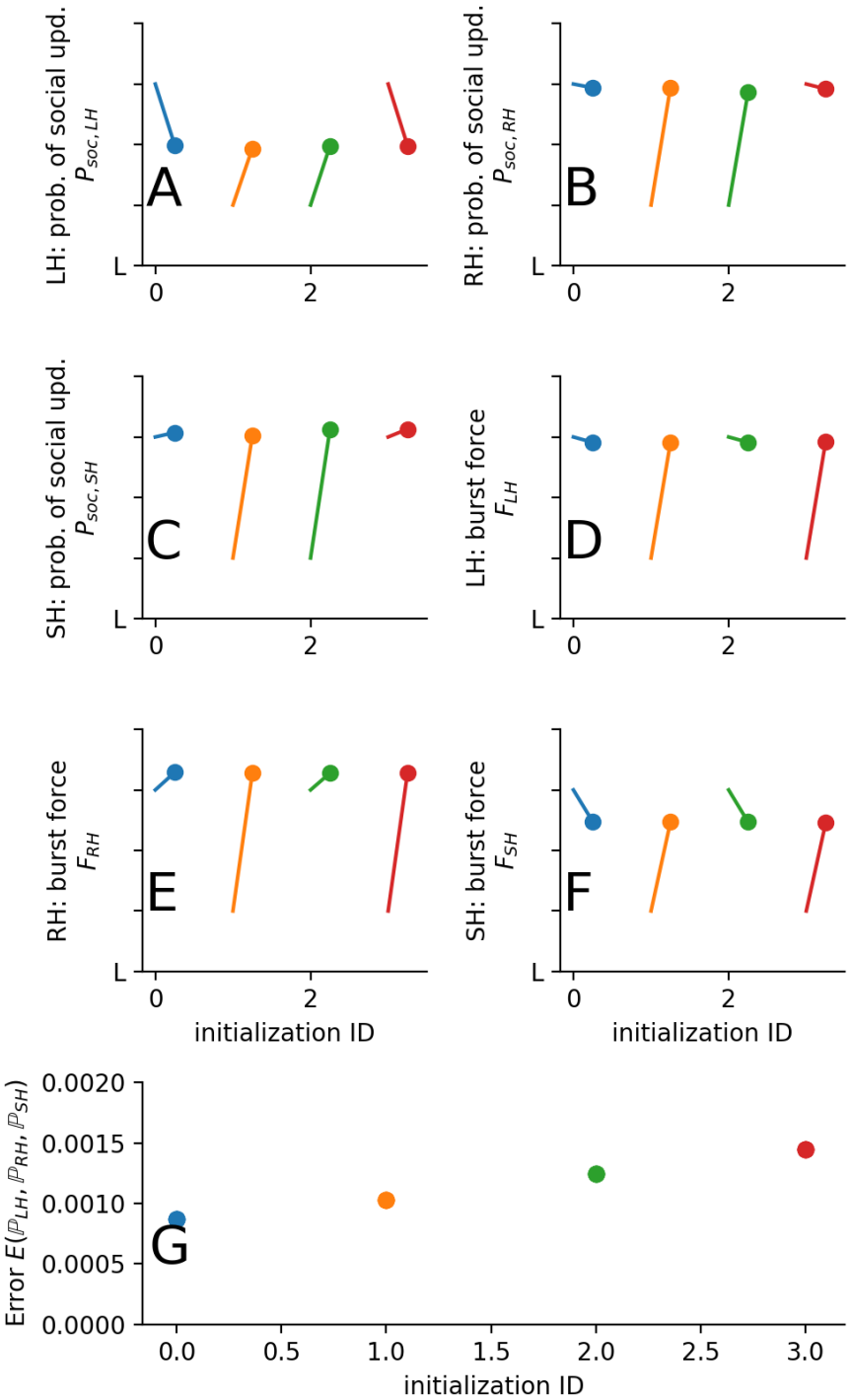

Fig. S9. Initial and final parameters (**A-F**) together with final error (**G**) according to Eq. S14 for the 4 different initialized optimization runs. The initialization are sorted such that the one with the best outcome, i.e. with the smallest error, is first. Colors mark specific initialization ID and are consistent across subfigures. The circles (**A-E**) mark the final parameter while the other end of the line marks the initial setting.

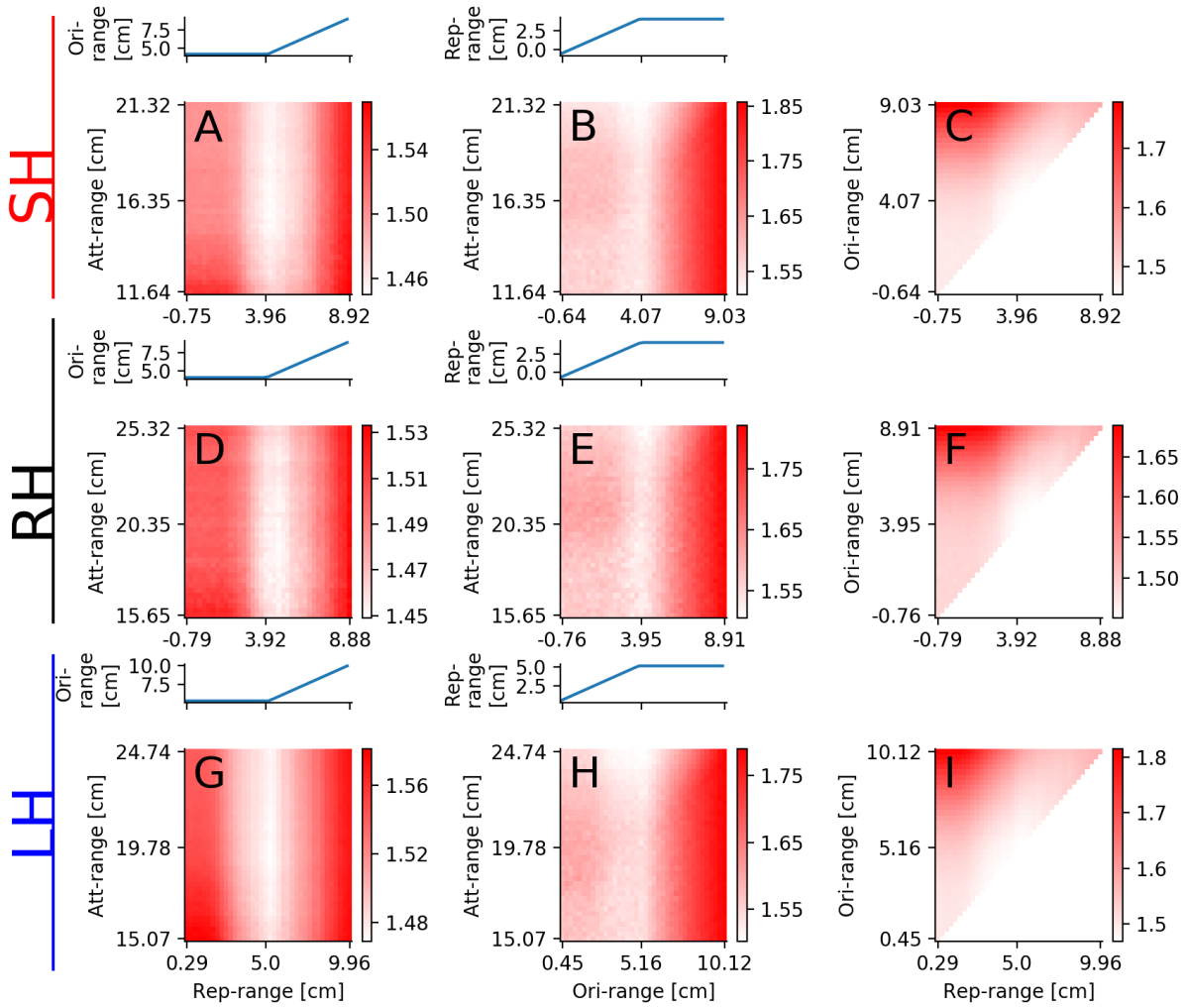

Fig. S10. Angle difference between predicted and actual direction after burst is color-coded. The difference is analyzed around the optimal values of the repulsion, orientation and attraction ranges. The line-plots above the color-plots show the remaining range which was kept constant if possible but needed to be in- or decreased to ensure the inequality $r_r < r_o < r_a$. In the first (**A, B, C**), second (**D, E, F**) and third (**G, H, I**) row is data used from burst-constellations of the small-, random- and large-harvested selection line, respectively. We varied the repulsion and attraction range in the first column (**A, D, G**), the orientation and attraction range in the second (**B, E, H**) and the repulsion and orientation range in the third column (**C, F, I**).

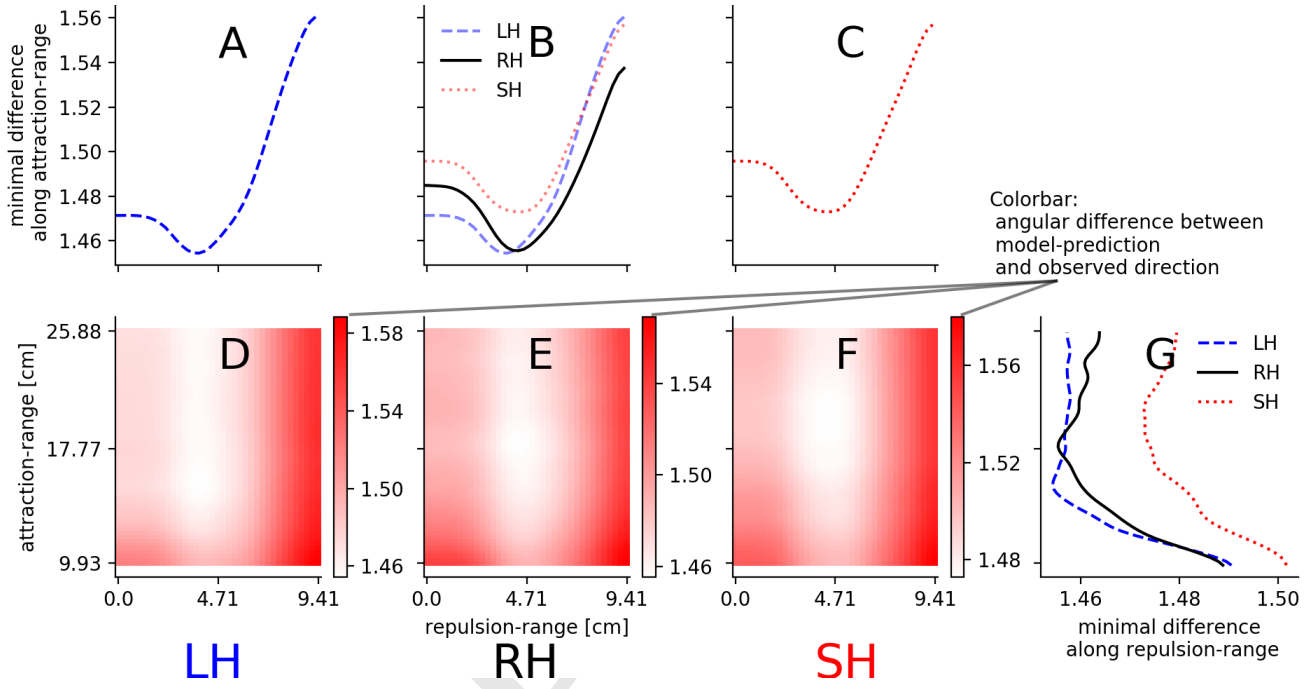

Fig. S11. Angle difference between predicted and actual direction after burst is color-coded (**D-F**) or its minimal value along one axis direction is shown (**A-C, G**). Here, in contrast to the scans in Fig.S10, no orientation-zone exists, i.e. $r_o = r_r$. **A-C**: minimal angle difference along the attraction-range is shown for burst-constellation data of the large- (**A**), small-harvest (**C**) and for all lines (**B**). **D-F**: angular difference for different parameters of repulsion and attraction range for the large-(**D**), random-(**E**) and small-harvested line(**F**). **G**: minimal difference for a specific attraction-range for all selection lines.

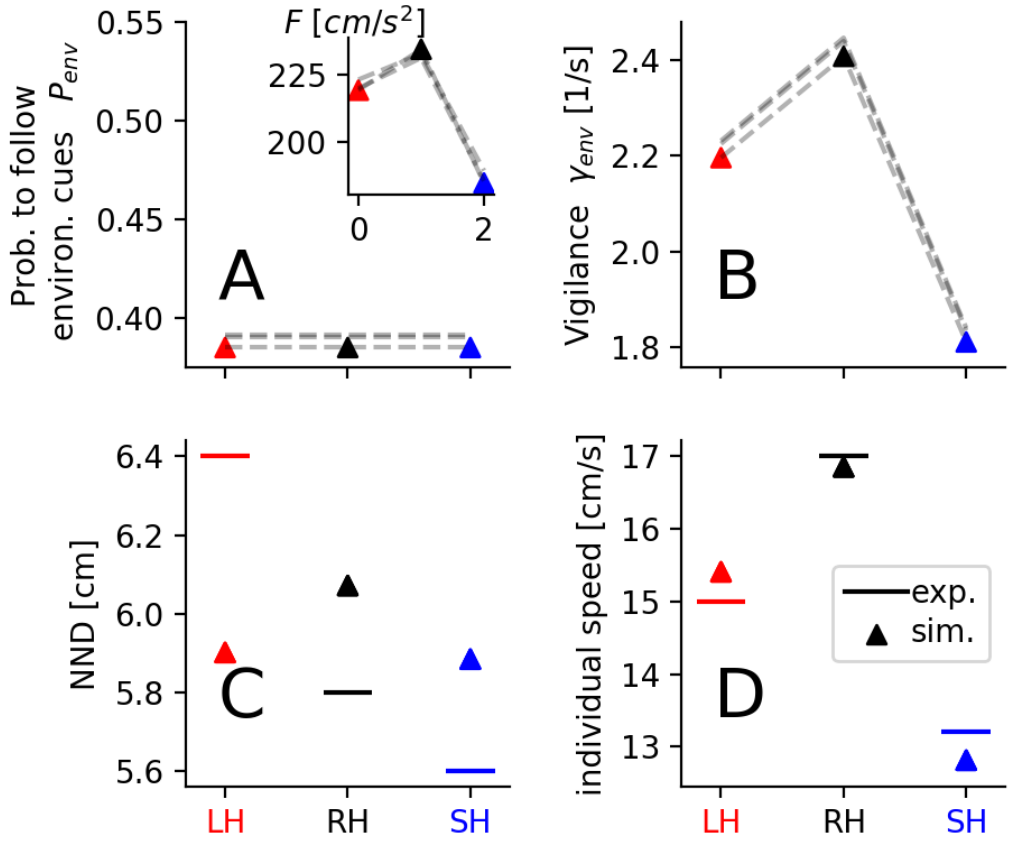

Fig. S12. Fitted model representation of the different selection lines. Note that here, in **contrast to Fig. 4 in the main text, we enforced the probability to follow environmental cues to be the same for all selection lines**. In order to resemble the experimental observations the probability to follow environmental cues (**A**) and the burst force (inset **A**) were set for each selection line. The vigilance γ_{env} is the product of P_{env} and the burst rate γ (**B**). The average nearest neighbor distance (NND, **C**) and the average individual speed (**D**) are emergent properties of the model and were used to quantify how well the parameters (P_{env}, γ) reproduce the experimental observations. In all panels: the triangles represent to the model parameters or the simulation outcomes of the parameter set with the best match to the experiment. Each dashed line (**A, B**) represents a parameter set of a different initialization, and therefore illustrates the robustness of the best matching parameter set (triangles). The horizontal solid lines (**C, D**) mark the experimental values. Note that in contrast to Fig. 3 units are in cm because the modelled agents have no body length. The selection lines are indicated by different colors (red=LH: large-harvested; black=RH: random-harvested; blue=SH: small-harvested).